



Ministério da
**Ciência, Tecnologia
e Inovação**



sid.inpe.br/mtc-m19/2013/03.25.17.57-TDI

ON DROPLET COMBUSTION: EFFECT OF MAGNETO RELAXATION HEATING

Cesar Flaubiano da Cruz Cristaldo

Doctorate Thesis Course Graduate
in Space Engineering and Tech-
nology/Combustion and Propul-
sion, advised by Dr. Fernando Fa-
chini Filho, approved in April 18,
2013.

URL of the original document:

<<http://urlib.net/8JMKD3MGP7W/3DQ4F2B>>

INPE
São José dos Campos
2013

PUBLISHED BY:

Instituto Nacional de Pesquisas Espaciais - INPE

Gabinete do Diretor (GB)

Serviço de Informação e Documentação (SID)

Caixa Postal 515 - CEP 12.245-970

São José dos Campos - SP - Brasil

Tel.:(012) 3208-6923/6921

Fax: (012) 3208-6919

E-mail: pubtc@sid.inpe.br

BOARD OF PUBLISHING AND PRESERVATION OF INPE INTELLECTUAL PRODUCTION (RE/DIR-204):**Chairperson:**

Marciana Leite Ribeiro - Serviço de Informação e Documentação (SID)

Members:

Dr. Antonio Fernando Bertachini de Almeida Prado - Coordenação Engenharia e Tecnologia Espacial (ETE)

Dr^a Inez Staciarini Batista - Coordenação Ciências Espaciais e Atmosféricas (CEA)

Dr. Gerald Jean Francis Banon - Coordenação Observação da Terra (OBT)

Dr. Germano de Souza Kienbaum - Centro de Tecnologias Especiais (CTE)

Dr. Manoel Alonso Gan - Centro de Previsão de Tempo e Estudos Climáticos (CPT)

Dr^a Maria do Carmo de Andrade Nono - Conselho de Pós-Graduação

Dr. Plínio Carlos Alvalá - Centro de Ciência do Sistema Terrestre (CST)

DIGITAL LIBRARY:

Dr. Gerald Jean Francis Banon - Coordenação de Observação da Terra (OBT)

DOCUMENT REVIEW:

Marciana Leite Ribeiro - Serviço de Informação e Documentação (SID)

Yolanda Ribeiro da Silva Souza - Serviço de Informação e Documentação (SID)

ELECTRONIC EDITING:

Maria Tereza Smith de Brito - Serviço de Informação e Documentação (SID)

Luciana Manacero - Serviço de Informação e Documentação (SID)



Ministério da
**Ciência, Tecnologia
e Inovação**



sid.inpe.br/mtc-m19/2013/03.25.17.57-TDI

ON DROPLET COMBUSTION: EFFECT OF MAGNETO RELAXATION HEATING

Cesar Flaubiano da Cruz Cristaldo

Doctorate Thesis Course Graduate
in Space Engineering and Tech-
nology/Combustion and Propul-
sion, advised by Dr. Fernando Fa-
chini Filho, approved in April 18,
2013.

URL of the original document:

<<http://urlib.net/8JMKD3MGP7W/3DQ4F2B>>

INPE
São José dos Campos
2013

Cataloging in Publication Data

Cristaldo, Cesar Flaubiano da Cruz.
C868d On droplet combustion: effect of magneto relaxation heating / Cesar Flaubiano da Cruz Cristaldo. – São José dos Campos : INPE, 2013.

xx + 67 p. ; (sid.inpe.br/mtc-m19/2013/03.25.17.57-TDI)

Thesis (Doctorate in Space Engineering and Technology/Combustion and Propulsion) – Instituto Nacional de Pesquisas Espaciais, São José dos Campos, 2013.

Adviser : Dr. Fernando Fachini Filho.

1. droplet combustion 2. magneto relaxation heating. 3. Brownian. 4. ferrofluid. I.Título.

CDU 536.423.1



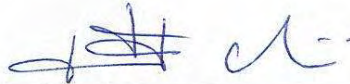
Esta obra foi licenciada sob uma Licença [Creative Commons Atribuição-NãoComercial 3.0 Não Adaptada](https://creativecommons.org/licenses/by-nc/3.0/).

This work is licensed under a [Creative Commons Attribution-NonCommercial 3.0 Unported License](https://creativecommons.org/licenses/by-nc/3.0/).

Aprovado (a) pela Banca Examinadora
em cumprimento ao requisito exigido para
obtenção do Título de **Doutor(a)** em

**Engenharia e Tecnologia
Espaciais/Combustão e Propulsão**

Dr. Fernando Fachini Filho



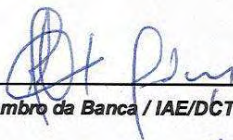
Presidente / Orientador(a) / INPE / Cachoeira Paulista - SP

Dr. Wladimir Mattos da Costa Dourado



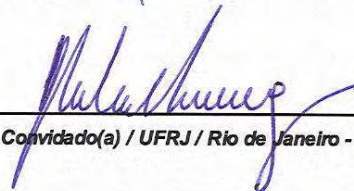
Membro da Banca / IAE/DCTA / São José dos Campos - SP

Dr. Marcio Teixeira de Mendonça



Membro da Banca / IAE/DCTA / SJCampos - SP

Dr. Albino Leiroz



Convidado(a) / UFRJ / Rio de Janeiro - RJ

Dr. Aldelio Bueno Caldeira



Convidado(a) / IME / Rio de Janeiro - RJ

Este trabalho foi aprovado por:

() maioria simples

(x) unanimidade

Aluno (a): **César Flaubiano da Cruz Cristaldo**

São José dos Campos, 18 de Abril de 2013

ACKNOWLEDGEMENTS

Agradeço primeiramente a Deus pelas oportunidades de crescimento que a vida nos proporciona.

Ao orientador Fernando Fachini Filho, pelo incentivo, compreensão e paciência. Obrigado, por me mostrar como trabalhar de forma séria e buscando, sempre, produzir pesquisa de alto nível.

Aos professores do INPE e ITA (Dr. João Luiz Filgueiras Azevedo) que contribuíram para minha formação, ao Dr. Álvaro Luiz de Bortoli (UFRGS) que me possibilitou chegar até aqui, ao Dr. Guilherme Coelho Cunha pelo suporte em métodos numéricos na última etapa do doutorado, aos professores Dr. Fernando Marcelo Pereira e Dr. Luc Bauwens que colaboraram na correção ortográfica dos 2 artigos publicados.

Aos colegas e funcionários do Laboratório de Combustão de Propulsão LCP/INPE pela convivência e amizade.

À Dra. Sin Chan Chou que me possibilitou adquirir novos conhecimentos no CPTEC/INPE.

Ao Conselho Nacional de Desenvolvimento Científico e Tecnológico - CNPQ proj. No. 142110/2009-4 e à Coordenação de Aperfeiçoamento de Pessoal de Nível superior - CAPES.

Agradeço a minha esposa pelo amor e companheirismo durante os momentos difíceis.

Agradeço a todos os amigos e familiares que, de alguma forma, contribuíram para o desenvolvimento deste trabalho. Pessoas que me incentivaram de diferentes maneiras. A todos vocês o meu sincero “muito obrigado”.

ABSTRACT

In this work, the influence of an external alternating magnetic field on heating, vaporization and combustion of a ferrofluid (liquid with dispersed magnetic nanoparticles) droplet is investigated. The response of the magnetic nanoparticles to the magnetic field generates heat inside the droplet, due to magneto relaxation, which acts as a heat source. This phenomenon is produced by friction (viscous dissipation) between rotating nanoparticles and the liquid surrounding them. The rotating motion of the nanoparticles is induced by the magnetic dipole fixed on each nanoparticle, which tends to align itself with the magnetic field. In the absence of magnetic field, Brownian motion of the liquid molecules is responsible for misaligning the dipoles, after collisions with the nanoparticle surface. Under the influence of an external alternating magnetic field, the process of aligning and misaligning repeats itself in each cycle, producing heat by viscous dissipation, due to a periodically reversing nanoparticle circular motion. In the present analysis the process of magneto relaxation heating, together with heat transfer from the ambient is studied. These two mechanisms (magnetic heating and heat flux from the gas-phase) contribute to droplet heating, hence increasing the vaporization rate of ferrofluid droplets. Assuming a very large magnetic power and a uniform distribution of nanoparticles, the droplet core is uniformly heated. A thermal boundary layer is established in the liquid-phase adjacent to the droplet surface due to heat flux from the ambient atmosphere. The temperature profile inside the thermal boundary layer is obtained in appropriate time and length scales. In the present model, the ferrofluid droplet is heated up to its boiling temperature in a very short time. Additionally, under certain conditions the temperature inside the thermal boundary layer can become higher than the temperature at the droplet surface. This leads to boiling occurs inside the droplet rather than at the surface, as in classical models. The temperature difference between the thermal boundary layer and the droplet surface results in an extra heat flux to the droplet surface, which increases the vaporization rate. Moreover, the results point out that the thermal boundary layer depends directly on the oxidant Lewis number but the vaporization rate reciprocally on it.

SOBRE COMBUSTÃO DE GOTAS: EFEITO DO AQUECIMENTO MAGNÉTICO

RESUMO

Neste trabalho é investigada a influência de um campo magnético externo alternado no aquecimento, vaporização e combustão de uma gota de ferrofluido (líquido com nanopartículas dispersadas). A resposta das nanopartículas ao campo magnético gera calor no interior da gota devido a relaxação magnética que atua como uma fonte de calor. Este fenômeno é produzido pelo atrito (dissipação viscosa) entre as nanopartículas, com movimento rotatório, e o fluido ao redor das partículas. O movimento de rotação é induzido pelo dipolo magnético fixo em cada nanopartícula, que tende a se alinhar na direção do campo magnético. Na ausência do campo magnético o movimento Browniano das moléculas do líquido é responsável pelo desalinhamento dos dipolos, após colisões com a superfície das nanopartículas. Sob a influência de um campo magnético externo alternado, os processos de alinhamento e desalinhamento são repetidos em cada ciclo, produzindo calor por dissipação viscosa devido ao movimento circular periódico e reverso das nanopartículas. Na presente análise, o processo de aquecimento por relaxação magnética, juntamente com o calor do ambiente é estudado. Estes dois mecanismos (aquecimento magnético e fluxo de calor do ambiente gasoso) contribuem para o aquecimento e o aumento da taxa de vaporização da gota de ferrofluido. Assumindo uma alta potência magnética e distribuição uniforme de nanopartículas, o interior da gota é aquecido uniformemente. Porém, uma camada limite térmica é estabelecida na fase líquida adjacente à superfície da gota devido ao fluxo de calor do ambiente. O perfil de temperatura no interior da camada limite térmica é obtido em escalas apropriadas de tempo e espacial. No presente modelo, a gota de ferrofluido é aquecida até sua temperatura de ebulição em um curto intervalo de tempo. Além disso, sob certas condições, a temperatura dentro da camada limite térmica torna-se maior que a temperatura na superfície da gota. Isto leva a gota a atingir a temperatura de ebulição no interior da gota e não na superfície, como descrito pelos modelos clássicos. A diferença de temperatura entre a camada limite térmica e a superfície da gota resulta num fluxo de calor extra para a superfície da gota, resultando num aumento da taxa de vaporização. Além disso, os resultados evidenciam que a camada limite térmica é proporcional ao número de Lewis do oxidante, porém a taxa de vaporização é inversamente proporcional ao número de Lewis.

LIST OF FIGURES

	<u>Pág.</u>
1.1	Examples of different burning regimes in spray combustion 3
2.1	(a) Magnetic nanoparticle without presence of magnetic field. (b) Magnetic nanoparticle with the presence of magnetic field. 14
3.1	Schematic representation of the temperature profile of the problem: (a) liquid and gas phases in spatial coordinate r . (b) liquid phase in spatial coordinate x and gas phase in spatial coordinate r 19
3.2	Dependence of the droplet properties on the frequency of the magnetic field at the time in which any part of the droplet reaches the boiling temperature: (a) heating time, (b) vaporization rate, (c) droplet surface temperature and (d) droplet radius, for three different ambient temperature. 24
3.3	Evolution of the temperature profile for three different magnetic field frequencies $f = 0.3$ (a), 1.0 (b) and 5.0 (c) for $\theta_\infty = 6.0$ 26
3.4	Droplet surface temperature as a function of time for three different magnetic field frequencies $f = 0.3$ (a), 1.0 (b) and 5.0 (c) for $\theta_\infty = 6.0$ 27
3.5	Vaporization rate as a function of time for three different magnetic field frequencies $f = 0.3$ (a), 1.0 (b) and 5.0 (c) for $\theta_\infty = 6.0$ 27
3.6	Evolution of the temperature profile for three different magnetic field frequencies $f = 0.3$ (a), 1.0 (b) and 5.0 (c) for $\theta_\infty = 1.0$ 29
3.7	Comparison of the results for the droplet surface temperature evolution from the present model and an analytical solution(FACHINI; BAKUZIS, 2010), for three different magnetic field frequencies $f = 0.3, 1.0, 5.0$ and ambient temperature $\theta_\infty = 1.0$ 30
3.8	Time evolution of the vaporization rate for three different magnetic field frequencies $f = 0.3, 1.0, 5.0$ and ambient temperature $\theta_\infty = 1.0$ 30
3.9	Comparison of the results for the evolution of the fuel mass fraction at the droplet surface from the present model and an analytical solution(FACHINI; BAKUZIS, 2010), for three different magnetic field frequencies $f = 0.3, 1.0, 5.0$ and ambient temperature $\theta_\infty = 1.0$ 31
3.10	Evolution of the temperature profile for three different magnetic field frequencies $f = 0.3$ (a), 1.0 (b) and 5.0 (c) and $\theta_\infty = 0.75$ 32

3.11	Heat flux across the droplet surface as a function of time for different magnetic field frequencies $f = 0.3, 1.0, 5.0$ under the conditions $\theta_\infty = 0.75, 1.0, 1.25$. ($q^- < 0$ represents heat loss from the droplet to the ambient atmosphere and $q^- > 0$ represents heat gain from the gas phase).	33
3.12	Time evolution for the square droplet radius for three different magnetic field frequencies $f = 0.3, 1.0, 5.0$, ambient temperature $\theta_\infty = 0.75$ and ambient fuel mass fraction $Y_\infty = 0.2$	34
3.13	Time evolution for the vaporization rate for three different magnetic field frequencies $f = 0.3, 1.0, 5.0$, ambient temperature $\theta_\infty = 0.75$ and ambient fuel mass fraction $Y_\infty = 0.2$	35
3.14	Time evolution of the temperature profile for three different values of the Lewis number $Le = 0.5$ (a), 1.0 (b) and 1.8 (c), magnetic field frequency $f = 5.0$ and ambient temperature $\theta_\infty = 6.0$.	36
3.15	Time evolution of the boundary layer thickness for three different Lewis number $Le = 0.5, 1.0$ and 1.8 , magnetic field frequency $f = 5.0$ and ambient temperature $\theta_\infty = 6.0$.	37
3.16	Time evolution of the vaporization rate for three different Lewis number $Le = 0.5, 1.0$ and 1.8 , magnetic field frequency $f = 5.0$ and ambient temperature $\theta_\infty = 6.0$.	38
3.17	Time evolution of the droplet surface temperature for three different Lewis number $Le = 0.5, 1.0$ and 1.8 , magnetic field frequency $f = 5.0$ and ambient temperature $\theta_\infty = 6.0$.	38
3.18	Temperature profiles for magnetic relaxation heating ($P_m = 1950$ and $f = 4$) and irradiated laser heating model (PARK; ARMSTRONG, 1989) at times, $t = 0.2, 0.4, 0.6, 0.8, 1.0, 1.2, 1.4 \mu s$.	40
4.1	Evolution of the droplet surface temperature as a function of time for $f \ll 1$ (comparison of analytical and numerical solutions).	48
4.2	Heating time τ_h as a function of magnetic field frequency for different values of Lewis number.	49
4.3	Temperature profile of ferrofluid droplet (n-heptane) for $f = 0.3$	50
4.4	Temperature profile of ferrofluid droplet (n-heptane) for $f = 1.0$	50
4.5	Temperature profile of ferrofluid droplet (n-heptane) for $f = 5.0$	51
4.6	Thermal boundary layer thickness as a function of the magnetic field frequency at the instant when boiling temperature is reached.	52
4.7	Vaporization rate as a function of magnetic field frequency at the instant when boiling temperature is reached.	53
4.8	Flame temperature as a function of magnetic field frequency at the instant when boiling temperature is reached.	54

4.9 Flame position as a function of magnetic field frequency at the instant
when boiling temperature is reached. 55

LIST OF SYMBOLS

a	–	droplet radius
A	–	$c_p k_l / c_l k_{g\infty}$
B	–	magnitude of magnetic induction
\mathbf{B}	–	magnetic induction
c	–	specific heat
E	–	electric field
E_{inc}	–	incident electric field
f	–	frequency
H	–	magnitude of magnetic field
\bar{H}	–	enthalpy
\mathbf{H}	–	magnetic field
H_0	–	magnetic field amplitude
I	–	laser power
$Im(\)$	–	imaginary component
k	–	thermal conductivity
L	–	latent heat
Le	–	Lewis number
L_{eff}	–	effective latent heat
\tilde{L}	–	Langevin equation
M	–	magnetization of material
\dot{m}	–	vaporization rate
M_d	–	magnetization domain
M_w	–	molecular weight
P	–	volumetric power dissipation
P_m	–	magnetic power parameter
P_L	–	laser power parameter
n	–	exponent of temperature
Q	–	combustion heat
\bar{Q}	–	heat
Q^-	–	heat flux to the liquid phase
q^-	–	$Q^- / (AP_m)^{1/2}$
r	–	radial coordinate
r_N	–	nanoparticle radius
$Re(\)$	–	real component
R_g	–	gas universal constant
s	–	$s_O Le_O / Le_F$
S	–	source term
S_L	–	$ E ^2 / E_{inc} ^2$
t	–	time
t_m	–	effective relaxation time

T	–	temperature
u	–	velocity
U	–	internal energy
V_N	–	nanoparticle volume
V_H	–	hydrodynamic volume
\bar{W}	–	magnetic work
Y	–	mass fraction
x	–	spatial coordinate for the thermal boundary layer
\bar{Z}	–	mixture fraction

Greek letters

α	–	thermal diffusivity
β	–	λ/a
γ	–	$L^*M_w/(R_gT_b^*)$
δ	–	thickness of the thermal boundary layer
δ_c	–	thickness of the coating layer
ϵ	–	ρ_∞/ρ_l
η	–	viscosity
θ	–	dimensionless temperature
κ	–	Boltzmann constant
λ	–	dimensional vaporization rate
λ_{tw}	–	wavelength
μ_0	–	magnetic permeability
ν	–	mass stoichiometric coefficient
ξ	–	Langevin parameter
ρ	–	density
τ	–	dimensionless time
τ_0	–	thermal fluctuation
ϕ	–	nanoparticles volume fraction
χ_0	–	equilibrium magnetic susceptibility
χ	–	magnetic susceptibility
χ'	–	real component of magnetic susceptibility
χ''	–	imaginary component of magnetic susceptibility
ω	–	consumption rate of species

Subscripts

b	–	boiling condition
B	–	Brownian mechanism
c	–	characteristic of the droplet
f	–	flame position

- F – fuel
- g – gas
- i – initial condition
- l – liquid
- N – Néel mechanism
- O – oxidant
- p – gas
- s – droplet surface
- ∞ – ambient atmosphere condition

Superscript

- * – dimensional property

CONTENTS

	<u>Pág.</u>
1 INTRODUCTION	1
1.0.1 Objectives	1
1.1 Spray combustion	2
1.2 Single droplet combustion	4
1.3 Nanofluids	6
1.3.0.1 Applications	6
1.4 Ferrofluids	7
1.4.1 Applications	7
1.5 Motivation	8
1.6 Thesis outline	9
2 MAGNETO RELAXATION HEATING	11
2.1 Power dissipation	11
2.2 Relaxation mechanism	13
2.3 Model hypothesis	14
3 HEATING AND VAPORIZATION	17
3.1 Mathematic formulation	17
3.2 Numerical strategy	22
3.3 Results and discussions	23
3.3.1 High ambient atmosphere temperature	25
3.3.2 Ambient atmosphere at boiling temperature	28
3.3.3 Low ambient atmosphere temperature	31
3.3.4 Low ambient atmosphere temperature with $Y_\infty = 0.2$	33
3.3.5 Influence of the Lewis number	35
3.4 Comparison of magnetic and laser heating	37
4 COMBUSTION PROBLEM	41
4.1 Model formulation	41
4.1.1 Numerical strategy	47
4.2 Results	47
5 CONCLUSION AND FUTURE WORKS	57

5.1	Conclusion	57
5.2	Future Works	58
	REFERENCES	61

1 INTRODUCTION

In this chapter, the objectives of the present work are presented. A complete and detailed description of all processes related to the droplet problem is presented in excellent published reviews (FAETH, 1977; LAW, 1982; SAZHIN, 2006). Hence, only an overview of the main processes directed related to the subject of this work are presented. An overview of the main characteristics of spray combustion and the importance of studies on single droplet are presented. Also, the main characteristics of nanofluids and ferrofluids with some of their applications are presented. Thereafter, the motivation of the present work is given.

1.0.1 Objectives

In this work, the magneto relaxation heating of ferrofluids under influence of an external alternating magnetic field is considered as an additional heat source in the droplet combustion problem (ROSENSWEIG, 2002; KAPPIYOOR et al., 2010). The magnetic nanoparticles dispersed inside the droplet acts as a heat source. The heating is produced by the energy dissipation due to friction between the rotating magnetic nanoparticles under the influence of an external magnetic field and the liquid surrounding them.

In previous work, the thermal problem of liquid phase of ferrofluid droplet exposed to external alternating magnetic field was investigated (FACHINI; BAKUZIS, 2010). Under the hypothesis of very large magnetic power, an analytical solution for droplet heating is obtained. This solution does not permit the description of temperature gradients inside the droplet imposed by heat flux from the gas phase. Under this condition, the coupling of the solutions of droplet liquid core and gas-phase is not possible.

In the present analysis, a model that describes gradients inside the droplet (thermal boundary layer) is formulated. From this model, the heating, vaporization and combustion are considered (CRISTALDO; FACHINI, 2013a; CRISTALDO; FACHINI, 2013b). From the droplet point of view, the interest is on the heating and vaporization imposed by both the magnetic process and the heat flux from gas phase. The conditions addressed in the problem consider a very larger magnetic power compared with the thermal power. As will be seen ahead, a thermal boundary layer is established in the liquid region adjacent to the droplet surface. Inside the thermal boundary layer, the magnetic and the thermal powers are of the same order, but in the droplet core the thermal power is negligible compared with the magnetic power.

The main contribution of this work is the thermal boundary layer formulation that describes the region adjacent to the ferrofluid droplet surface. This formulation allows to match the solution of the droplet core to that of the gas-phase.

1.1 Spray combustion

Spray combustion has long been a major engineering concern, and efforts have been made to achieve high efficiency with better control of pollutants in combustion products. However, due to the complex nature of spray combustion processes, many practical devices were designed based upon the trial-and-error approach, which is very expensive (KUO, 1986). Performance and design of combustion chamber are mainly influenced by the injection velocity and vaporization rate of the liquid fuel. Due to the nature of liquids, these properties of the liquid fuel in combustion chambers are directly related to the atomization process.

Since combustion occurs in the gas phase, liquid fuels must be vaporized before burning. The energy required for the liquid fuel vaporization is supplied by the heat transferred from the flame or ambient atmosphere to the fuel (LORELL et al., 1956), which is a function of the temperature gradient and surface area. The gradient of temperature is imposed by the temperature difference between the ambient atmosphere, whose value is close to the flame temperature, and liquid surface, whose value is close to the boiling temperature. Thus, the gradient of temperature close to the droplet is almost a constant property inside combustion chambers. However, the contact surface between the liquid phase and the gaseous phase is a property that can change by many orders of magnitude via atomization. Therefore, the atomization is the process controlling the combustion of liquid, namely spray combustion.

The spray may be produced through atomization of a liquid jet issuing from a simple cylindrical nozzle or more complex injectors. The atomization may be considered as a result of several contributing factors such as, turbulence in the liquid jet, cavitation in the nozzle, aerodynamic shear stresses between the liquid jet and the surrounding gaseous medium. Near field of injector, a dense region of droplets having various sizes might occur, whilst in the far field, a dilute region of more uniform size droplets might form.

One attempt to model spray combustion is to consider the spray like a spherical cloud of droplets. In this context, different burning regimes may occur, since a region of dense cloud to a dilute spray region (see fig. 1.1). In dense region, a cloud of droplets is surrounded by a flame. This cloud can contain an internal region (cold

region) of non-evaporating droplets. In intermediate configuration, isolated burning droplets take place in the external region of a cloud of evaporating droplets. Inside the cloud, a droplet cannot be treated as if it were an isolated droplet. In this case, the droplet is influenced by neighboring droplets and, to some extent, by all droplets in the spray.

In a dilute region, the droplets are far apart from each other, consequently the influence of neighboring droplets becomes negligible. In this configuration flames enclosing each droplet, as shown in fig. 1.1.

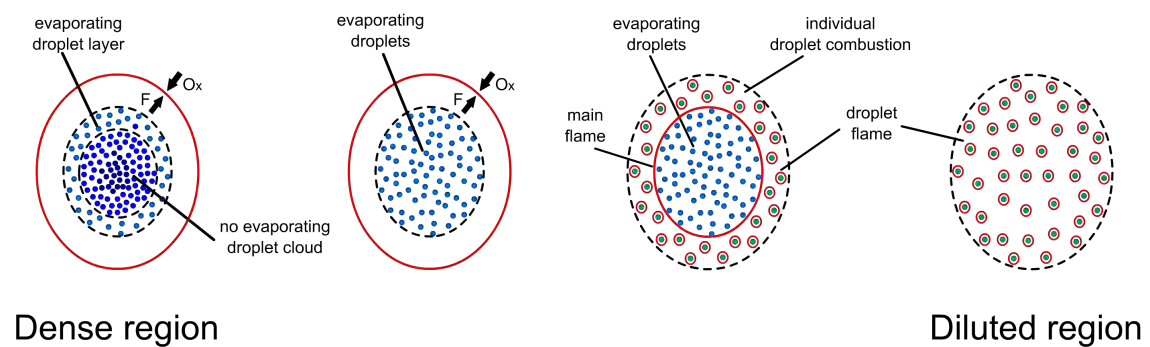


Figure 1.1 - Examples of different burning regimes in spray combustion

The governing equations describing the droplets cloud are similar to those describing a single droplet. This fact allows expecting analogies between single droplet combustion and droplet cloud combustion on different time and length scales. This analogy frequently serves as a useful methodology to look into spray combustion characteristics (UMEMURA, 1994). This is the motivation for several assumptions in the development of the single droplet vaporization models.

In addition, the study of a single droplet is an important step in developing models that may be used to predict and improve the performance of many combustion devices (FAETH, 1977; LAW, 1982; SIRIGNANO, 1983; SAZHIN, 2006). For instance, the determination of the droplet lifetime is an important property in combustion-chamber design. The droplet lifetime and the droplet velocity in sprays determine the minimum time the droplet must be allowed to reside in the combustion chamber and, hence, the length of the combustion chamber (SIRIGNANO, 1999). Also, due to the high cost of numerical simulation of spray problems with their multiple scales, sub-models of isolated droplet are developed to be employed in the description of droplet scales processes in simulation codes.

1.2 Single droplet combustion

The classical theory of vaporization and combustion of fuel droplets is based for low Reynolds numbers, when the effects of the motion of the droplet relative to the ambient atmosphere can be neglected (GODSAVE, 1953; SPALDING, 1953; WISE; ABLOW, 1957). Neglecting the relative motion is perfectly justified for droplets in practical devices, for instance, diesel engines, which allows the consideration of all processes in the liquid phase as well as in the gas phase to be spherico-symmetric. Under these assumptions, a spherical diffusion flame surrounding the droplet is established with the mass transfer of two reactants interdiffusing from opposite directions. One of these reactants is originated at the surface of the droplet, while the source of the other is located in the gas phase at an infinite distance relative to the liquid droplet. As a result of an exothermic chemical interaction between the two reactants, the diffusion flame is established at some distance from the droplet surface. The basic droplet combustion model was formulated by GODSAVE (1953) and SPALDING (1953) for a single fuel droplet burning in a stagnant oxidizing environment. According to GODSAVE (1953), two distinct mechanisms may be recognized as determining the vaporization rates of the droplet in a liquid fuel spray during the processes of vaporization and combustion. The first mechanism occurs when the temperature of ambient atmosphere is the same as that of the individual droplet. The temperature is still low compared to the boiling point of the fuel. Under these conditions the vaporization rate is determined by mass diffusion. The predominant parameter in this case is the vapor pressure of the liquid. The second mechanism occurs when the ambient temperature is high in relation to the droplet temperature. In this case vaporization rate is determined by heat flux from the gas phase to the liquid phase. Meanwhile the temperature of the droplet is below the boiling temperature, part of the heat transferred to the droplet is to heat it up and the other part is to vaporize the droplet (GODSAVE, 1953; SPALDING, 1953).

In the spray context, the mechanism, in which the vaporization rate is controlled by vapor pressure of liquid (low ambient temperature), is found close to the fuel injection in which the spray is dense and the gas phase temperature is low. The mechanism, in which the vaporization rate is controlled by heat flux from the gas-phase (high ambient temperature), occurs in regions close to spray border in which droplets are sufficiently far apart from each other (at a distance of about 20 times the droplet diameter) and the droplet eventually is surrounded by the flame.

The thermal problem of the droplet can be modeled in different ways: constant

temperature, infinite conductivity, finity conductivity, vortex model and effective conductivity. The simplest model is the one considering the assumption of constant droplet temperature equal to the boiling temperature (KOTAKE; OKAZAKI, 1969). This implies that the heat flux to the droplet is totally employed to vaporize it (SIRIGNANO, 1983). The constant temperature condition is found for low volatile fuels, for which the droplet heating is practically separated from the droplet vaporization at constant droplet temperature (WISE; ABLOW, 1957).

The infinite conductivity model is based on the assumption that the thermal conductivity of the liquid is very high and the temperature gradients inside the droplets can be ignored, but is temporally varying (WILLIAMS, 1960). The finite thermal conductivity model provides the detail description for the heating process of a droplet (temperature gradients inside the droplet) (LAW; SIRIGNANO, 1977). The model describes the non-uniform temperature evolution inside the droplet, with a transient-conduction equation.

Generally, the droplet lifetime predicted by the finite conductivity model is shorter than that predicted by the infinite conductivity model. The reason for that is the droplet radius to be evaluated based on the droplet surface temperature, which is higher than the interior temperature during the droplet heating and vaporization. Also, the finite conductivity model represents the experimental results better than the infinite conductivity model (BALASUBRAMANYAM et al., 2007).

The vortex model is appropriated to describe droplet problems with relative velocity to the gas phase. The shear stress between gas flow and the droplet surface induces a recirculation movement inside the droplet. For a not too large Reynolds number, a vortex is generated inside the droplet. The recirculation causes a significant decrease in the characteristic length and time for the liquid-phase heat and mass transfer (SIRIGNANO, 1983).

The effective conductivity model is a simplification of the vortex model. It is considered as an artificial thermal conductivity in the finite conductivity model in order to take into account the recirculation within the droplet (PRAKASH; SIRIGNANO, 1978; PRAKASH; SIRIGNANO, 1980; ABRAMZOM; SIRIGNANO, 1983).

As can be seen above, several models were developed to describe the heating and vaporization processes of the droplets. All efforts devoted to model the heating and vaporization processes are a strong evidence of their importance on design of combustion chambers (SIRIGNANO, 1999). Recently nanofluids and ferrofluids appear

as a new topics of research in spray combustion. They provide improvements in the heat transfer in liquids which has a significant change in heating and vaporization of droplets (ROSENSWEIG, 1985; ODENBACH, 2002; SHLIOMIS, 2003; SARIT et al., 2007; ODENBACH, 2009).

1.3 Nanofluids

Fluids containing suspension of nanoparticles (nanofluids) have been extensively studied due to their enhanced physical properties, e.g. viscosity, specific heat and thermal conductivity (ROSENSWEIG, 2002; WEN et al., 2009; WONG; LEON, 2010). The large number of nanofluid applications have demanded understanding of their properties and modeling. In the context of thermal problems, various theoretical models have been proposed for explaining the exceptional increase in the thermal conductivity. Empirical expressions for the effective thermal conductivity were proposed based on the thermal conductivities of the solid and liquid, their respective volume fractions and the nanoparticle size (XUAN, 2000; XUAN; ROETZEL, 2000; XUE, 2003). More accurate models include effects of the nanoparticle-fluid interaction (nanolayer) (WANG, 2003; FENG et al., 2007). Since liquid molecules close to the nanoparticle surface form layered structures that behave much like a solid, the thermal conductivity increases. One possible explanation for the existence of the nanolayer is that the molecular structure of the liquid is more ordered in that region. Thus, a higher local thermal conductivity is expected in the liquid near the interface of the nanoparticle (YU, 2003; TILLMAN; HILL, 2007; ZHANG; MA, 2008).

1.3.0.1 Applications

In recent years, nanofluids are been used in the automotive industry in various applications such as coolant, fuel additives and lubricant. Specifically, improvements in heat transfer are obtained due to the replacement of water with nanofluids in the automobile radiator (PEYGHAMBARZADEH et al., 2011). The results show that the concentration of nanoparticle plays an important role in the heat transfer efficiency. By the addition of 1% vol. of Al_2O_3 nanoparticles into pure water, an increase of about 30-45 % of the heat transfer coefficient in comparison with the pure water is observed (PEYGHAMBARZADEH et al., 2011). In addition, the use of high thermal conductivity of the nanofluids in radiators can lead to a reduction in the frontal area of the radiator by up to 10% (SINGH et al., 2006).

In combustion devices, the burning of nanofluids has been an active field of research. Significant changes in some combustion properties, such as reduction on the fuel

heating and vaporization times and on the pollutant emissions, have been observed. Also, a simple experiment of dropping a diesel droplet on a high temperature surface shows that the presence of nanoparticles is responsible for reducing the ignition time (TYAGI et al., 2008). The effect of aqueous aluminum nanoparticles in compression ignition engine has also been investigated. The aluminum nanoparticles have very high activity and can react with water at temperatures from 673.15 K to 873.15 K to generate hydrogen which helps the flame stability (JUNG et al., 2008; RAJA et al., 2011). In addition, the aluminum nanoparticles serve as a catalyst to decompose water (JUNG et al., 2008).

1.4 Ferrofluids

Nanofluids can present magnetic properties if magnetic nanoparticles are dispersed into the base liquid. These are known as magnetic nanofluids or ferrofluids (BLUMS et al., 1998; SHLIOMIS, 2003; VÖLKER; ODENBACH, 2003; VEKAS, 2007; ONDECK et al., 2009). The advantage of ferrofluids over non-magnetic nanofluids is the wide range of applications that can be controlled by the frequency, amplitude and direction of external magnetic field.

1.4.1 Applications

Recently, the addition of magnetic nanoparticles in fuels (ferrofluid) has been explored (GAN; QIAO, 2011a; GAN; QIAO, 2011b). The performance of a diesel engine with water-based ferrofluid was investigated. Results indicate an increase in thermal efficiency up to 12% and a decrease in specific fuel consumption up to 11% as compared to diesel fuel. Moreover, the advantage of the ferrofluid is that the magnetic nanoparticles possibly may be collected (in the gas phase) at the exhaust flow by a magnetic bar (SHAFII et al., 2011).

In presence of a stationary magnetic field, the magnetic nanoparticles align their dipoles with magnetic field and stay still even in shear flows, with a consequent increase in the viscosity (ROSENSWEIG, 1985; SHLIOMIS, 2003). Another work, the ferrofluid being exposed to an external magnetic field gradient is attracted to the region of the highest intensity field (PLAZA et al., 2000). Thus, ferrofluid flow can be driven by the motion of the magnetic field. An application for that is to pump a secondary fluid or to carry a body immersed in a ferrofluid (HATCH et al., 2001; YAMAHATA et al., 2005; FELDERHOF, 2011). Another application is the rupture of the ferrofluid droplets into microdroplets by applying a uniform magnetic field. The magnetic field induces perturbations on the droplet surface, known as Rosenweig

instability, that are responsible to break it up. Then, the magnetic field can be adjusted to control the final size of the micro-droplets (CHEN; LI, 2010). These ideas can also be applied to improve the spray atomization process.

In 1957, the heat generated by interaction of magnetic nanoparticles with an external alternating magnetic field was suggested as a method for cancer treatment (GILCHRST et al., 1957). In this mechanism, the cancerous cells are destroyed by increasing the temperature of tumor cells (ROSENSWEIG, 2002; KAPPIYOOR et al., 2010). This mechanism is known as magnetic hyperthermia or magneto relaxation heating, which is the heat generated by the response of the magnetic nanoparticles to the alternating magnetic field. Due to its complexity, even after 50 years, the magnetic heating has not become part of a clinical practice. But recent progress in the preparation of magnetic nanoparticles and the improved physical understanding of their interaction with external magnetic fields has been achieved (ODENBACH, 2009). Today, the magneto relaxation heating is a promising modality for cancer treatment.

In this work, a new application for the magneto relaxation heating is proposed: the acceleration of the heating process of droplets (FACHINI; BAKUZIS, 2010).

1.5 Motivation

As mentioned, atomization is the key process in heating, vaporization and burning of liquid fuels, because the heat flux from gas phase to the droplets is directly dependent on the total spray liquid-gas interface area (FAETH, 1977; SIRIGNANO, 1983; SAZHIN, 2006). Of course, the density number of droplets in sprays, another property established by atomization rather than droplet surface area, is to be considered because it controls the local temperature inside sprays, which has a direct influence on the heat flux to the droplets. However, since the stoichiometric fuel-air ratio for the most used fuels from heat generation to transport by surface and air is very small, the mean number density has no significant influence. Then, without any other heat source, the heating, vaporization and burning processes are determined by the atomization.

The characteristic times of heating, vaporization, mixture and burning have direct influence on the droplet residence time in a chamber combustion. In order to reduce the droplet heating and vaporization times, a new heat source (ferrofluid under the influence of external alternating magnetic field) is added within the droplet via process of magnetic relaxation heating. Thus a shorter chamber combustion can be designed.

1.6 Thesis outline

In chapter 2, a brief discussion of the magnetic source is exhibited. The physical process of heat generation by magneto relaxation heat is presented in detail.

In chapter 3, the effect of magneto relaxation heating of a ferrofluid fuel droplet is analyzed under the condition of very large magnetic power. The ferrofluid droplet is in a quiescent inert gas phase with a temperature which is set equal to, higher and lower than the liquid boiling temperature. The results are obtained in appropriate time and length scales, which are imposed by the thermal boundary layer established in the liquid-phase adjacent to the droplet surface.

The results for different magnetic field frequencies are discussed in terms of temperature profiles in the thermal boundary layer, time evolution of the droplet surface temperature, vaporization rate, fuel mass fraction at droplet surface, heat flux across the droplet surface, droplet radius and boundary layer thickness. Also, a parametric study of Lewis number is made in the heating process. At the end of this chapter the magneto relaxation heating of ferrofluid droplet (water-maghemite) is compared with the heating of pure water droplet irradiated by an unpolarized plane wave CO_2 laser beam.

In chapter 4, the combustion process is included in the previous analysis. In this new condition, the magneto relaxation heating together with heat flux from the flame contribute to the droplet heating and increase the vaporization rate of ferrofluid droplets. Like semi-transparent droplets absorbing heat from the flame by radiation (TSENG; VISKANTA, 2006), a thermal boundary layer is formed in the liquid on the droplet surface. The results are discussed for the following properties: heating time, temperature profile, thermal boundary layer thickness, vaporization rate, flame temperature and flame position.

Chapter 5 summarises the thesis and offers some conclusions and suggestions for future research.

2 MAGNETO RELAXATION HEATING

2.1 Power dissipation

Under the application of an external alternating magnetic field the energy that is absorbed by the ferrofluid is transferred to the surrounding liquid in the form of heat. This mechanism is known as magnetic hyperthermia (for medical applications) or magneto relaxation heating. A crucial factor in magneto relaxation heating is the power P absorbed by the magnetic nanoparticles per volume via orientational relaxation of the magnetic dipole in a magnetic field of amplitude H_0^* and frequency f^* . Hereafter, the process of power dissipation is presented and quantified (ROSENSWEIG, 2002).

From the first law of thermodynamics for a constant density system of unit volume the following equation for the conservation of energy is given

$$dU^* = \delta\bar{Q}^* + \delta\bar{W}^* \quad (2.1)$$

in which U^* is the internal energy, \bar{Q}^* the heat added and \bar{W}^* the magnetic work done on the system. For an adiabatic process $\delta\bar{Q}^* = 0$ with the differential magnetic work per unit volume, given in general by $\delta\bar{W}^* = \mathbf{H}^* \cdot d\mathbf{B}^*$, Equation (2.1) is rewritten as

$$dU^* = \mathbf{H}^* \cdot d\mathbf{B}^* \quad (2.2)$$

in which \mathbf{H}^* ($A\ m^{-1}$) is the magnetic field intensity and \mathbf{B}^* (*Tesla*) is the induction. In the present case, \mathbf{H} and \mathbf{B} are collinear, which is the case for isotropic material in a time-steady field. Therefore the scalar product $\mathbf{H}^* \cdot d\mathbf{B}^*$ is expressed in terms of the field magnitude as $dU^* = H^* \cdot dB^*$. The magnetic induction is represented by $B^* = \mu_0(H^* + M^*)$, in which M^* ($A\ m^{-1}$) is the material magnetization and $\mu_0 = 4\pi \times 10^{-7}$ ($T\ m\ A^{-1}$) is the magnetic permeability. Integrating Eq. 2.2 and replacing B^* , one finds an increase of internal energy per cycle according to

$$\Delta U^* = -\mu_0 \oint M^* dH^*. \quad (2.3)$$

When magnetization lags the field, the integration yields a positive result, indicating a change of magnetic work into internal energy. It will be convenient to express the magnetization in terms of the complex ferrofluid susceptibility χ , that is a measure of how sensitive a material is to an applied field. The magnetic susceptibility is represented by real and imaginary components $\chi = \chi' - i\chi''$. The imaginary com-

ponent of the susceptibility is equivalent to the energy released as heat. The applied magnetic field is given by

$$H^*(t^*) = H_0^* \cos(2\pi f^* t^*). \quad (2.4)$$

H_0^* is the amplitude of magnetic field. The nanoparticle magnetization is given by

$$M^*(t^*) = H_0^* [\chi' \cos(2\pi f^* t^*) + \chi'' \sin(2\pi f^* t^*)] \quad (2.5)$$

in which χ' is the in-phase component, χ'' is the out-phase component of χ and t^* is the time. Substituting $M^*(t^*)$ and $H^*(t^*)$ in Eq. (2.3) leads to

$$\Delta U^* = 2\mu_0 H_0^{*2} \chi'' \int_0^{1/f^*} \sin^2(2\pi f^* t^*) dt^*, \quad (2.6)$$

As seen in Eq. (2.6), the internal energy variation is a function only of the imaginary component χ'' (energy released as heat). Integrating and multiplying the result by the cyclic frequency f^* , the following expression for volumetric power dissipation is found

$$P = f^* \Delta U^* = \mu_0 \pi \chi'' f^* H_0^{*2}. \quad (2.7)$$

The volumetric power dissipation $P(Wm^{-3})$ is related to specific power loss (Wg^{-1}) by the mean mass density of nanoparticles. To make use of this result, χ'' must be related to material parameters of the ferrofluid. The magnetization equation was derived phenomenologically (ROSENSWEIG, 1985) as a modification of the Debye relaxation equation (DEBYEG, 1929),

$$\frac{dM^*(t^*)}{dt^*} = -\frac{M^*(t^*) - M_0^*(t^*)}{t_m^*} \quad (2.8)$$

in which t_m^* is the relaxation time and $M_0^*(t^*)$ is the equilibrium magnetization given by

$$M_0^*(t^*) = \chi_0 H_0^* \cos(2\pi f^* t^*). \quad (2.9)$$

The equilibrium magnetic susceptibility is described as $\chi_0^* = 3\chi_i^* \tilde{L}(\xi)/\xi$ in which the initial susceptibility is defined as $\chi_i^* \equiv \mu_0^* \phi M_d^2 V_N^*/(3\kappa T^*)$, with ϕ and M_d being the volume fraction of nanoparticles and the domain magnetization, respectively. The function $\tilde{L}(\xi)$ is known as Langevin function and is defined as $\tilde{L}(\xi) = \coth \xi - 1/\xi$, in which $\xi \equiv \mu_0^* M_d V_N^* H^*(t^*)/(\kappa T^*)$. This function treats a particle as an integral over the energy of all individual magnetic moments, which are in thermal equilibrium at temperature T^* with an energy distribution according

to Boltzmann. The magnetic susceptibility χ_0^* can be considered as a mean value based on the applied magnetic field ($H^* \approx H_0^*$) (ROSENSWEIG, 2002).

Replacing Eqs. (2.5) and (2.9) into Eq. (2.8), results in

$$\chi = \frac{\chi_0^*}{1 + i2\pi f^* t_m^*} \quad (2.10)$$

which gives the dependence of complex susceptibility on frequency. The components of susceptibility are

$$\chi' = \frac{\chi_0^*}{1 + (2\pi f^* t_m^*)^2} \quad (2.11)$$

and

$$\chi'' = \frac{\chi_0^* 2\pi f^* t_m^*}{1 + (2\pi f^* t_m^*)^2}. \quad (2.12)$$

Equation 2.12 is related to magnetic losses. These relationships (Eqs. 2.11 and 2.12) are identical to the Debye spectra of polar molecules in the absence of a constant magnetic field. Replacing Eq. (2.12) into Eq. (2.7) results in the following expression for volumetric power dissipation from nanoparticles under an alternating magnetic field of amplitude H_0^* and frequency f^* (ROSENSWEIG, 2002)

$$P = \mu_0 \pi \chi_0^* H_0^{*2} \frac{2\pi f^{*2} t_m^*}{1 + (2\pi f^* t_m^*)^2}. \quad (2.13)$$

2.2 Relaxation mechanism

Magnetic nanoparticles dispersed in a fuel droplet are subjected to an external alternating magnetic field. The nanoparticles dipoles align themselves with the magnetic field (ROSENSWEIG, 1985). In the absence of magnetic field, however, under Brownian motion, fuel molecules collide with the nanoparticles, leading to misalignment of the magnetic dipoles 2.1-a. As a result, the nanoparticles rotative motion against the surrounding liquid generates heat by friction 2.1-b (ROSENSWEIG, 2002).

This heat generation process is known as magneto Brownian relaxation heat source. Heat generation can also be achieved by a second mechanism, known as Néel relaxation. In that mechanism the nanoparticle remains stationary and the dipole rotates within the nanoparticle crystal structure, causing an increase of the nanoparticle temperature. The Néel relaxation mechanism is significant at very high frequencies. In the present analysis, however, the period of the external magnetic field is taken to be of the order of the droplet heating time, resulting in frequencies much below

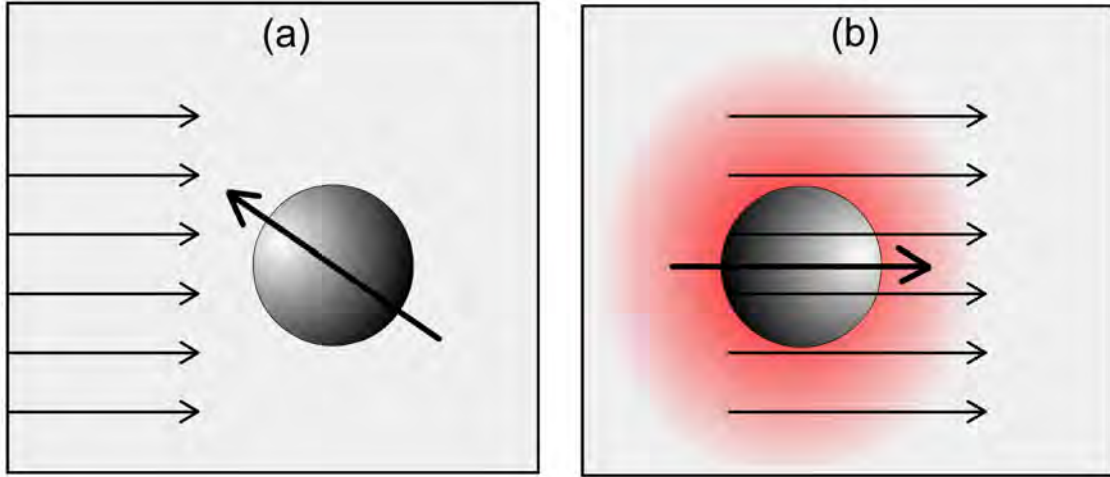


Figure 2.1 - (a) Magnetic nanoparticle without presence of magnetic field. (b) Magnetic nanoparticle with the presence of magnetic field.

the range at which that mechanism becomes important.

The effective relaxation time is defined by

$$\frac{1}{t_m^*(T^*)} = \frac{1}{t_B^*(T^*)} + \frac{1}{t_N^*(T^*)}, \quad (2.14)$$

in which $t_B^*(T^*)$ and $t_N^*(T^*)$ are Brownian and Néel relaxation times, respectively. As seen, the faster relaxation mechanism dominates heat generation. Relaxation times depend upon temperature T^* according to $t_B^*(T^*) \equiv 3\eta V_H^*/(\kappa T^*)$ and $t_N^*(T^*) = \tau_0 \exp(\Gamma)[\pi/(4\Gamma)]^{1/2}$ (ROSENSWEIG, 1985). The parameter Γ is a function of temperature given by $\Gamma \equiv KV_N^*/(\kappa T^*)$, in which K is the anisotropy constant, V_N^* is the volume of the magnetic nanoparticle and $\kappa = 1.39 \times 10^{-23}$ J/K is the Boltzmann constant. The other properties are: the average relaxation time in response to a thermal fluctuation τ_0 , the viscosity of the medium η and the hydrodynamic volume of magnetic nanoparticles V_H^* . In the present analysis, as mentioned above, the heating process is dominated by the Brownian relaxation mechanism, $t_B^*(T^*) \ll t_N^*(T^*)$, then $t_m^*(T^*) = t_B^*(T^*)$. Generally, that assumption is valid for fluids with low viscosity (ONDECK et al., 2009), which is accurate for many fuels.

2.3 Model hypothesis

The main objective of this study is to determine the effect of magneto Brownian relaxation heating on the burning of ferrofluid fuel droplets. Although changes of fluid properties (e.g. viscosity, thermal conductivity, density and specific heat) due

to the presence of nanoparticles are important, they are not taken into account. For instance, addition of 7% in volume of nanoparticles increases about 8% the ferrofluid specific heat per volume, $(\rho_l c_l)_{eff}$, and an increase of about 20% in the thermal conductivity (XUE, 2003; CHANDRASEKAR et al., 2010). The thermodynamic and transport properties used in the simulation will be the same as the liquid fuel, as mentioned. The influence of the thermodynamic and transport properties will be examined in future works. The aim of these assumptions is to highlight only the influence of the magnetic heating on the droplet heating.

Indeed their effect are small compared to magneto heating in the conditions under consideration in this analysis: magnetic heat source much larger than thermal heat source (under the notation below, $P_m \gg 1$).

Since the main interest of this work is on the fundamental of magnetic heating applying on droplets, feasible practical cases, costs and overall energy balance will be examined in other works.

The nanoparticles distribution inside the droplet is considered uniform in the present analysis. For a high magnetic heat source compared with the one provided by the heat flux from the gas-phase, the temperature inside the droplet is uniform (FACHINI; BAKUZIS, 2010). In the region close to the droplet surface, both heat sources, magnetic relaxation and the one provided by the heat flux from gas phase, have the same intensity. Consequently, a thermal boundary layer is established in that region during the droplet heating process. To follow the evolution of the thermal boundary layer, it is necessary to rescale the spatial and time coordinates. The solution for the thermal boundary layer matches the solution of the droplet core to that of the gas-phase, which is quasi-steady.

The Brownian motion of nanoparticles and the regression of the droplet surface can cause agglomeration of nanoparticles on the droplet surface during the vaporization (GAN; QIAO, 2011a). However, the agglomeration process is not taken into account in this analysis, as will be proved ahead.

3 HEATING AND VAPORIZATION

In this section the ferrofluid droplet is placed in a quiescent ambient atmosphere at different temperatures. For vaporization without combustion the presence of oxidant in the environment is irrelevant. For droplet temperature below the ambient atmosphere, heat is transferred to the droplet. At the surface, part of this heat is further transferred to the droplet interior causing the droplet to heat up. The rest is used to vaporize the liquid such that a high concentration of fuel vapor, generally at its saturation value, exists at the droplet surface. Otherwise, heat is transported from the droplet to the ambient atmosphere if the initial temperature of the droplet is greater than the temperature of the ambient atmosphere.

3.1 Mathematic formulation

Whereas the ferrofluid droplet is in a quiescent ambient atmosphere, all processes in the liquid and gas phases present spherical symmetry and the problem can be considered as one-dimensional. The liquid phase presents the following properties: density ρ_l , specific heat c_l and thermal conductivity k_l , which are considered constant. In a region far from the droplet surface, the following properties are constant: density ρ_∞^* , temperature T_∞^* , specific heat at constant pressure c_p and thermal conductivity k_{g_∞} . The liquid and gaseous phases are described by conservation equations, which are written in terms of the following nondimensional variables,

$$t \equiv \frac{t^*}{t_c^*}, \quad r \equiv \frac{r^*}{a^*(0)}, \quad \rho \equiv \frac{\rho^*}{\rho_\infty^*},$$

$$\theta \equiv \frac{T^*}{T_b^*}, \quad u \equiv \frac{u^* a^*(0)}{\alpha_\infty}, \quad \text{and} \quad a \equiv \frac{a^*}{a^*(0)},$$

in which t , r , ρ , θ , u and a represent time, radial coordinate, density, temperature, gas velocity and droplet radius, respectively. The superscript $*$ stands for variables in dimensional form and the subscripts b and ∞ stand for boiling and ambient conditions (far from the droplet), respectively. The time t^* is nondimensionalized by an estimated heating time $t_c^* \equiv [(a^*(0))^2 / (\alpha_\infty \epsilon)]$, with $\epsilon \equiv \rho_\infty^* / \rho_l^*$ and thermal diffusivity $\alpha_\infty \equiv k_{g_\infty} / c_p \rho_\infty^*$.

The conservation equations for mass and energy in the liquid phase are given by (FACHINI; BAKUZIS, 2010)

$$\frac{d}{dt}(a^3) = -3\lambda \tag{3.1}$$

and

$$\frac{\partial \theta}{\partial t} - \frac{A}{r^2} \frac{\partial}{\partial r} \left(r^2 \frac{\partial \theta}{\partial r} \right) = P_m \frac{f^2 t_m(\theta)}{1 + (f t_m(\theta))^2}, \quad (3.2)$$

in which $\lambda(t) \equiv \dot{m}(t^*)c_p/(4\pi k_{g\infty} a^*(0))$ is the dimensionless vaporization rate, $\dot{m}(t^*)$ is the dimensional vaporization rate and $A \equiv c_p k_l / c_l k_{g\infty}$. The right hand side of Eq. (3.2) represents the energy dissipation (Eq. 2.13) from magnetic nanoparticles under the influence of an alternating magnetic field (ROSENSWEIG, 2002). In the present model, the parameters that control the energy dissipation are the magnetic field frequency $f \equiv 2\pi f^* t_{B_b}^*$, $t_m \equiv t_m^*/t_{B_b}^*$ and the ratio of the magnetic heat source to the thermal source P_m . The frequency f^* is nondimensionalized by the effective relaxation time determined at the boiling temperature $t_{B_b}^*$. The magnetic parameter P_m is defined as (FACHINI; BAKUZIS, 2010)

$$P_m \equiv \frac{\mu_0 \chi_0 H_0^2 / 2}{\rho_l c_l T_b^*} \frac{t_c^*}{t_{B_b}^*}, \quad (3.3)$$

in which μ_0 is the magnetic permeability ($\mu_0 = 4\pi \times 10^{-7} \text{ T m/A}$), H_0 is the magnetic field amplitude, and the magnetic susceptibility χ_0 is described by Langevin equation

$$\chi_0 = \chi_i \frac{3}{\xi} \left(\coth \xi - \frac{1}{\xi} \right). \quad (3.4)$$

The initial susceptibility is given by $\chi_i \equiv \mu_0 \phi M_d^2 V_N / (3\kappa T^*)$, in which ϕ , M_d , V_N and κ are volume fraction of nanoparticles, domain magnetization, nanoparticles volume and Boltzmann constant ($1.38 \times 10^{-23} \text{ J/K}$), respectively. The Langevin parameter ξ is defined as $\xi = \mu_0 M_d H V_N / (\kappa T^*)$ with $H = H_0 \cos(2\pi f^* t^*)$. The equilibrium susceptibility χ_0 is a conservative estimative for low limit of the source term in Eq. (3.2) (ROSENSWEIG, 2002). Therefore, χ_0 can be assumed constant. This assumption is valid because the volume fraction of nanoparticles is constant during the heating period, as will be seen ahead. The Brownian relaxation time is related to the inverse of the temperature and is defined as $t_B^* \equiv 3\eta V_H / \kappa T^*$, where η is the viscosity of the surrounding liquid, and V_H is the hydrodynamic volume of the particle. The hydrodynamic volume is the effective volume that includes the volume of the coating layer of the nanoparticle. The Brownian relaxation time t_B^* is nondimensionalized by its value at the boiling temperature, leading to $t_B \equiv t_B^*/t_{B_b}^* = 1/\theta$ (FACHINI; BAKUZIS, 2010).

The hypothesis that the magnetic power is much larger than the thermal power, $P_m \gg 1$, is assumed in this work. This assumption is valid for a field intensity of about 10^{-2} Tesla. Under this condition, the temperature profile is uniform in the

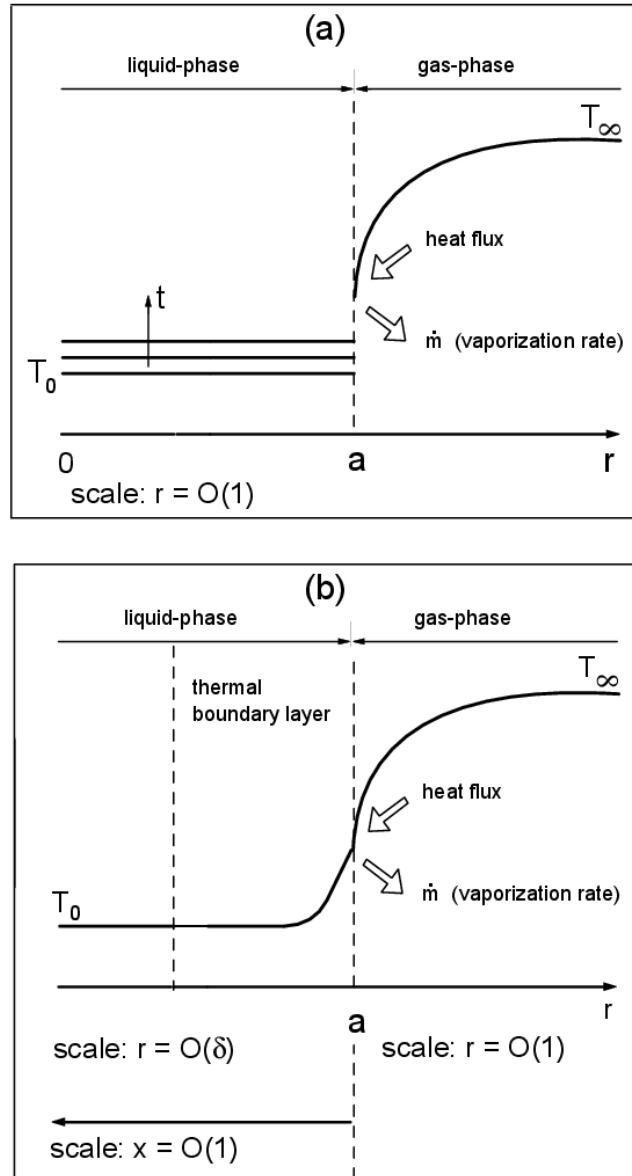


Figure 3.1 - Schematic representation of the temperature profile of the problem: (a) liquid and gas phases in spatial coordinate r . (b) liquid phase in spatial coordinate x and gas phase in spatial coordinate r .

droplet core, varying just with time (Fig. 3.1-a) (FACHINI; BAKUZIS, 2010). However, in a thin zone adjacent to the droplet surface, the uniform behavior from the temperature profile of the droplet core changes to a time-spatial variation to match the temperature gradient imposed by the heat flux from the gas-phase (Fig. 3.1-b). Consequently, a thermal boundary layer must be formed adjacent to the droplet surface. Therefore it is necessary to rescale not only the time but also the radial coordinate in Eqs. (3.1) and (3.2) to follow properly the evolution of the thermal boundary layer.

By analyzing Eq. (3.2), the appropriate time scale is $t \sim P_m^{-1}$, then the new time scale can be written as $\tau \equiv tP_m$, for $\tau = O(1)$. In addition, in order to describe the spatial variation of the temperature profile in the liquid phase, the following change of the spatial variable $r = a + \delta x$ is necessary. As will be shown, the thickness δ is very small, $\delta \sim P_m^{-1/2} \ll 1$. According to classical procedure, a thermal boundary layer is established in the thickness δ , which is described by the variable $x = O(1)$, as exhibited in the schematic Fig. 3.1-b.

Equations (3.1) and (3.2) in these new variables are written as:

$$\frac{d}{d\tau}(a^3) = -3\frac{\lambda}{P_m} \quad (3.5)$$

and

$$\frac{\partial\theta}{\partial\tau} + \frac{1}{\delta}\frac{da}{d\tau}\frac{\partial\theta}{\partial x} - \frac{A}{\delta^2 P_m}\frac{\partial^2\theta}{\partial x^2} = \frac{f^2\theta}{\theta^2 + f^2}. \quad (3.6)$$

By analyzing asymptotically the source term $S(\theta; f) \equiv f^2\theta/(f^2 + \theta^2)$, it is observed that $S(\theta; f) \sim f^2/\theta \ll 1$ and $S(\theta; f) \sim \theta$ for low ($f \ll 1$) and high ($f \gg 1$) frequencies, respectively. For $\delta = (A/P_m)^{1/2}$, all terms in Eq. (3.6) become of order unity, except the convective term, that presents the order $(AP_m)^{-1/2} \ll 1$ because $da/d\tau \sim P_m^{-1}$ for $a \sim 1$. Therefore, the effect of the convection due to the variation of the radius is negligible whereas $a \gg P_m^{-1/2}$ according to Eq. (3.5).

Thus, by imposing $\delta = (A/P_m)^{1/2}$, Eq. (3.6) takes the form

$$\frac{\partial\theta}{\partial\tau} - \frac{\partial^2\theta}{\partial x^2} = \frac{f^2\theta}{\theta^2 + f^2}. \quad (3.7)$$

This equation and the following boundary conditions

$$\frac{\partial\theta}{\partial x} = 0 \quad \text{for } x \rightarrow -\infty \quad (3.8)$$

and

$$a^2\theta^n \frac{\partial\theta}{\partial r} \Big|_{a^+} = (AP_m)^{1/2} a^2 \frac{\partial\theta}{\partial x} \Big|_{x=0^-} + \lambda L \quad \text{at } r = a, \quad (3.9)$$

describe the evolution of the temperature profile inside the thermal boundary layer. In this analysis, the gas thermal conductivity is considered to be a function of temperature, according to $k_g/k_{g\infty} = \theta^n$ with $n = 0.5$ (FACHINI; LINÁN, 1999). The dimensionless latent heat of vaporization is defined as $L \equiv L^*/(c_p T_b)$, where L^* is the latent heat of vaporization. Equation (3.9) represents the energy conservation at the droplet surface: part of the heat that is supplied by the ambient atmosphere

to the droplet is used for the droplet heating and part for the vaporization process.

Based on the gas phase radial flow from the droplet to the ambient atmosphere, the gas-phase conservation equations are presented below (FACHINI, 1999; FACHINI; LINÁN, 1999):

$$\epsilon P_m \frac{\partial \rho}{\partial \tau} + \frac{1}{r^2} \frac{\partial}{\partial r} (r^2 \rho u) = 0, \quad (3.10)$$

$$\epsilon P_m \rho \frac{\partial Y}{\partial \tau} + \rho u \frac{\partial Y}{\partial r} - \frac{1}{r^2} \frac{\partial}{\partial r} \left(\frac{r^2 \theta^n}{Le} \frac{\partial Y}{\partial r} \right) = 0, \quad (3.11)$$

$$\epsilon P_m \rho \frac{\partial \theta}{\partial \tau} + \rho u \frac{\partial \theta}{\partial r} - \frac{1}{r^2} \frac{\partial}{\partial r} \left(r^2 \theta^n \frac{\partial \theta}{\partial r} \right) = 0, \quad (3.12)$$

in which Y is the vapor mass fraction and Le is the vapor Lewis number. In this work, under low pressure conditions, $\epsilon \equiv \rho_\infty / \rho_l$ is considered small enough, such that the condition $\epsilon P_m \ll 1$ is still found. Hence, the gas phase processes can be treated as quasi-steady-state. Thus the conservation equations can be rewritten as

$$r^2 \rho u = \lambda, \quad (3.13)$$

$$\frac{\lambda}{r^2} \frac{\partial Y}{\partial r} - \frac{1}{r^2} \frac{\partial}{\partial r} \left(\frac{r^2 \theta^n}{Le} \frac{\partial Y}{\partial r} \right) = 0, \quad (3.14)$$

$$\frac{\lambda}{r^2} \frac{\partial \theta}{\partial r} - \frac{1}{r^2} \frac{\partial}{\partial r} \left(r^2 \theta^n \frac{\partial \theta}{\partial r} \right) = 0. \quad (3.15)$$

The boundary conditions at the surface are described by Eq.(3.9) and

$$-\frac{r^2 \theta^n}{Le} \frac{\partial Y}{\partial r} = \lambda(1 - Y_s), \quad \text{at } r = a^+. \quad (3.16)$$

The superscript $+$ stands for the condition at the surface in the gas-side and Y_s is the vapor mass fraction at the droplet surface. In the region far from the droplet, the following boundary conditions hold

$$\theta = \theta_\infty, \quad \text{and } Y = 0 \quad \text{as } r \rightarrow \infty. \quad (3.17)$$

At the liquid-gas interface, vapor and liquid are assumed to be in equilibrium. For this reason, the Clausius-Clapeyron relation

$$Y_s = \exp[\gamma(1 - \theta_b / \theta_s)] \quad (3.18)$$

can be used to relate the vapor mass fraction at the surface to the surface tem-

perature θ_s , where $\gamma \equiv L^*M_w/(R_gT_b^*)$ depends on the liquid molecular weight M_w and universal gas constant R_g . Equations (3.14) and (3.15) can be integrated once considering the boundary conditions given by Eqs. (3.16), (3.17) and the energy conservation at the interface, Eq.(3.9), resulting in the following system

$$\frac{\partial\theta}{\partial r} = \frac{\lambda(\theta - \theta_s + L) + Q^-}{r^2\theta^n}, \quad (3.19)$$

$$\frac{\partial Y}{\partial r} = -\frac{\lambda(1 - Y)Le}{r^2\theta^n}, \quad (3.20)$$

in which $Q^- \equiv (AP_m)^{1/2}a^2(\partial\theta/\partial x)_{x=0^-}$ is the heat flux from the surface to the inner region of the droplet.

3.2 Numerical strategy

A ferrofluid droplet with initial radius $a_0 = 1$ is in a quiescent inert atmosphere at temperature θ_∞ and vapor mass fraction Y_∞ . An alternating magnetic field is applied with frequency f . In this problem, the term ‘‘ambient temperature’’ means the temperature of a region far from the droplet. It is worth mentioning that the spatial scale of the liquid phase inside the thermal boundary layer is $r = O(\delta)$ or $x = O(1)$, and the gas phase is solved in the scale $r = O(1)$. For the numerical solution of the problem the following procedure is employed:

- 1) First, the energy conservation equation for the liquid phase, Eq.(3.7), is integrated with arbitrary values for the surface temperature θ_s and vaporization rate λ and, as a result, Q^- is calculated.
- 2) Using these values of θ_s , λ and Q^- , the integration of Eqs. (3.19) and (3.20) is performed from the droplet surface $r = a$ to a region far from the droplet $r \gg 1$.
- 3) If the boundary conditions θ_∞ and Y_∞ are not satisfied, new estimates for θ_s and λ are obtained by the Newton-Raphson procedure and the process is repeated until the boundary conditions are satisfied.
- 4) At this point, the process is advanced to the next time step.

Besides that, at each time step, the droplet radius is calculated using Eq. (3.5). According to this equation, the radius has a very small variation in $\tau = O(1)$. Even for $P_m \gg 1$, the vaporization rate λ is of the order unity because the heat flux from gas phase is order unity, as shown in Eq. (3.9). Therefore the heating process occurs practically with no expressive variation of the droplet radius. This justifies

the volume fraction of magnetic nanoparticles to be considered constant during the heating process.

3.3 Results and discussions

The base fluid used in this work is n-heptane at initial temperature of $297K$ or $\theta = 0.8$. The constants properties of the n-heptane are: density $\rho_l = 6.8 \times 10^5 \text{ g/m}^3$, thermal conductivity $k_l = 0.609 \text{ J/(m s K)}$, specific heat $c_l = 2.216 \text{ J/(g K)}$, latent heat of vaporization 316.76 J/g , boiling temperature $T_b^* = 371.15 \text{ K}$. The magnetic nanoparticle is maghemite ($\gamma\text{Fe}_2\text{O}_3$) of radius $r_N = 10 \text{ nm}$, thickness of coating layer $\delta_c = 1 \text{ nm}$, domain magnetization of $M_d = 414 \text{ kA/m}$ and volume fraction of nanoparticles $\phi = 0.07$. The magnetic induction $B_0 = \mu_0 H_0$ is 1 Tesla. The model demands $P_m \gg 1$, then the results presented ahead are for droplet radius larger than $70 \mu\text{m}$. For these properties the parameter P_m is 100. However, for $a < 70 \mu\text{m}$, P_m decreases according to $P_m/100 \sim (a/70)^2$ with droplet radius. For example, for $a = 10 \mu\text{m}$, P_m is about 2, such condition demands the integration of Eq. (3.2) to describe the temperature evolution, the boundary layer approximation is no longer valid.

The heating process is followed until any part of the droplet reaches the boiling temperature $\theta = 1$. This model does not allow the temperature in the droplet to be higher than the boiling temperature because any disturbance can generate bubbles in its interior and break it up. For all cases, the vapor mass fraction in the region far from the droplet is $Y_\infty = 0$ and the Lewis number Le is equal to unity, except when another value is explicitly mentioned.

It is important to highlight that, under certain conditions, the magnetic source may heat up the droplet core and/or the thermal boundary layer faster than the droplet surface is heated by the surrounding gas. Then, a heat flux from the droplet interior to the droplet surface must be observed. The consequences are higher vaporization rates as well as a local maximum for the temperature profile located inside the thermal boundary layer. Hence, the boiling condition is achieved not at the droplet surface but inside the thermal boundary layer. The numerical simulation is ended when the boiling temperature ($\theta = 1$) is achieved in any position of the droplet. Figure 3.2-a shows the heating time of the droplet as a function of the magnetic field frequency f for different values of ambient temperature θ_∞ . The frequency f varies from $f = 0.3$ to values for which the relaxation process of nanoparticles reaches the saturation state, $f \approx 5$. It is worth mentioning that, for $f < 0.3$, the model of the thermal boundary layer becomes unrealistic because its thickness becomes close

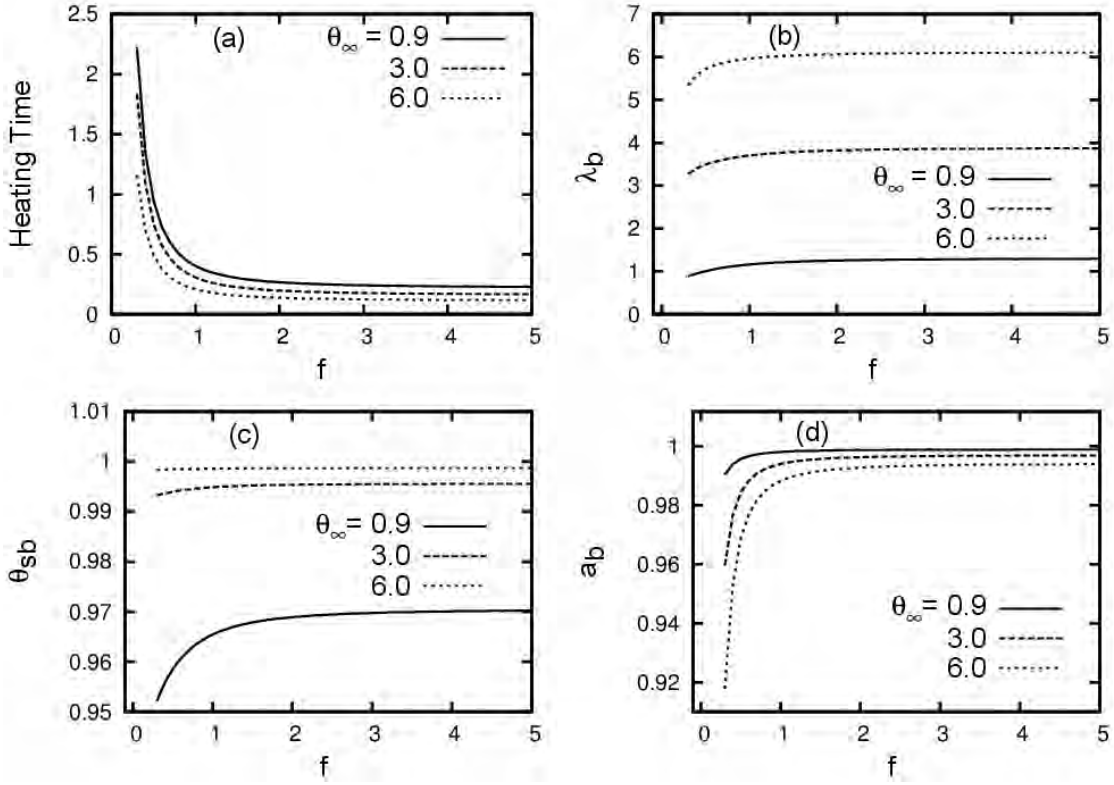


Figure 3.2 - Dependence of the droplet properties on the frequency of the magnetic field at the time in which any part of the droplet reaches the boiling temperature: (a) heating time, (b) vaporization rate, (c) droplet surface temperature and (d) droplet radius, for three different ambient temperature.

to one order of magnitude larger than $(A/P_m)^{1/2}$, precisely $\delta = (A/P_m)^{1/2}/f$, as pointed by Eq. (3.6). Since the magnetic source $S(\theta, f)$ increases with f , an increase of the magnetic field frequency reduces the time for the droplet to reach its boiling temperature. The pronounced influence of the ambient temperature on the heating time for low frequencies ($f < 1.5$) is observed. For high frequencies, however, the ambient temperature has little influence on the heating time, as seen in Fig. 3.2-a.

Figure 3.2-b shows the vaporization rate λ_b as a function of the magnetic field frequency. The subscript b from now on will stand for the variable value when any part of the droplet reaches the boiling condition. Unlike the droplet heating time, the frequency of the magnetic field does not have an expressive influence on the vaporization rate, as seen in Fig 3.2-b. Thus the vaporization rate is strongly dependent on the ambient temperature. Therefore, even for very intense magnetic heating, the vaporization rate keeps depending on the heat flux from the gas-phase, which explains the strong dependence on the ambient temperature.

Figure 3.2-c shows the temperature at the droplet surface θ_{sb} as a function of the magnetic field frequency f . Like the vaporization rate, the droplet surface temperature is strongly dependent on the ambient temperature. For the condition of low ambient temperature and low frequencies ($f < 1.5$), as shown in Fig. 3.2-c for $\theta_\infty = 0.9$, the magnetic field frequency also plays an important role in determining θ_{sb} .

Since the vaporization rate as well as the droplet surface temperature are controlled by the heat conservation at a very thin zone around the liquid-gas interface (droplet surface), the volumetric heat generation is negligible because of its dependence on the volume. This feature explain the strong dependence of the heating time with magnetic heating via the frequency and of the vaporization rate and droplet surface temperature with the heat flux from the gas-phase via the ambient temperature.

Figure 3.2-d shows the droplet radius a_b as a function of the magnetic field frequency using the same conditions as in the three previous plots. Since the heating time ($\tau = O(1)$) is very short, as seen in Fig. 3.2-a, the variation of the droplet radius during the heating time is very small. According to Eq. (3.5), it follows the relation $a_b^3 \sim 1 - 3\lambda/P_m$, a trend confirmed by Fig. 3.2-d. For low frequencies, the ambient temperature is responsible, through the ambient heat flux, for the increase of the vaporization rate and consequently the reduction of the droplet radius, hence a_b is smaller, the larger the ambient temperature θ_∞ is. From Fig. 3.2, it is concluded that the magneto relaxation heating has a strong influence on the heating time but weak on the vaporization rate.

Next, the droplet heating by magnetic heating process is analyzed at different ambient atmosphere conditions, temperature and vapor mass fraction.

3.3.1 High ambient atmosphere temperature

This section analyzes heating and vaporization of droplet in an ambient atmosphere of $\theta_\infty = 6$ and $Y_{F_\infty} = 0$. These values describe the ambient atmosphere with high temperature, no oxidant (inert environment) and low fuel mass fraction found by droplets close to flames, due to the spray combustion. The effects of the magnetic source are quantified in the cases $f = 0.3, 1.0$ and 5.0 . As can be seen in Fig. 3.3, the temperature inside the droplet becomes higher than that at the droplet surface. Therefore the temperature reaches the boiling condition inside the thermal boundary layer. This happens because, besides the magnetic heat source, the ambient heat flux is large enough to sustain high temperature in the thermal boundary layer even with

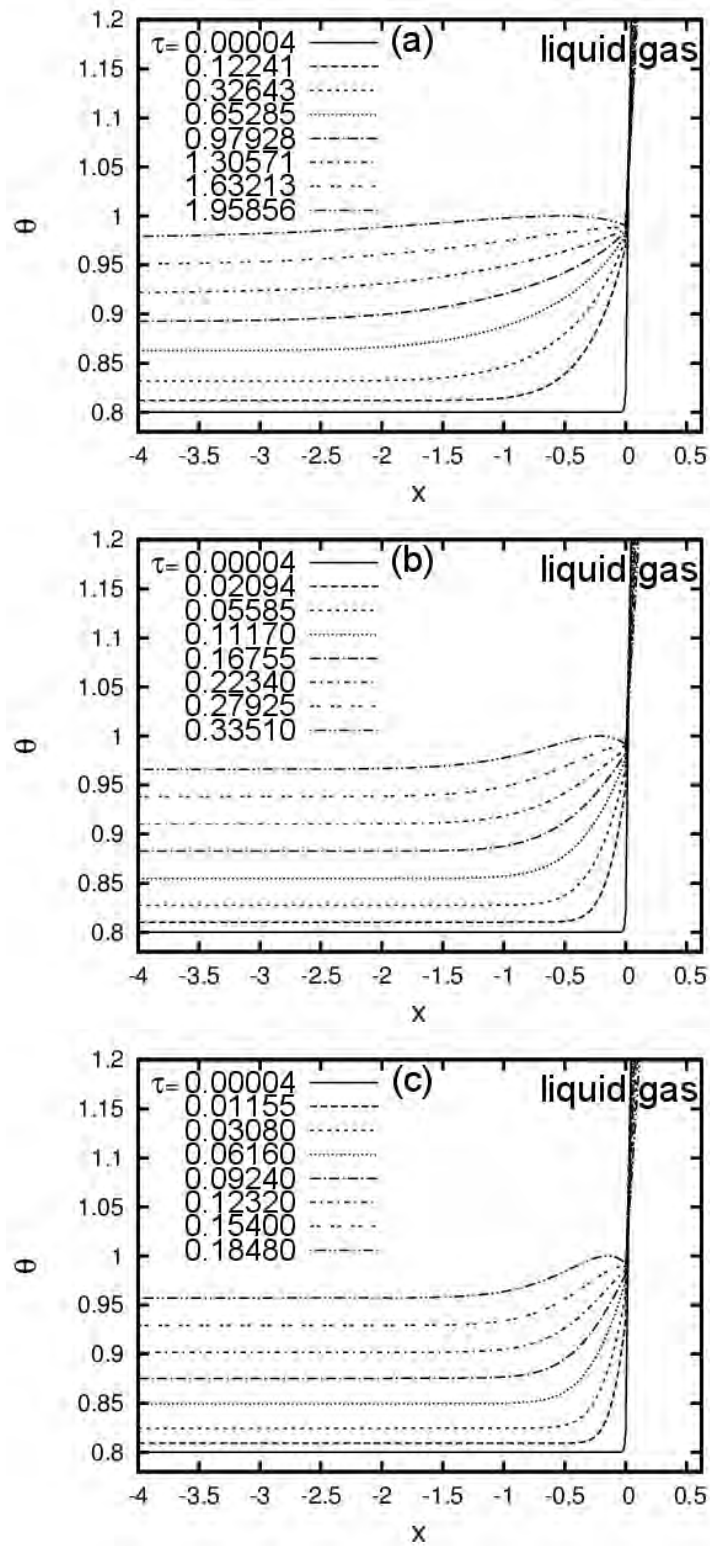


Figure 3.3 - Evolution of the temperature profile for three different magnetic field frequencies $f = 0.3$ (a), 1.0 (b) and 5.0 (c) for $\theta_\infty = 6.0$.

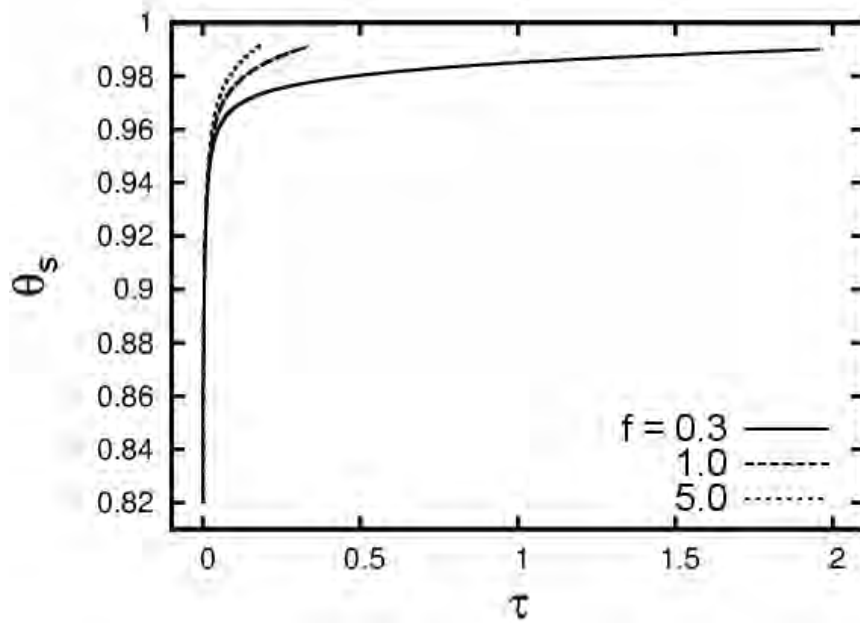


Figure 3.4 - Droplet surface temperature as a function of time for three different magnetic field frequencies $f = 0.3$ (a), 1.0 (b) and 5.0 (c) for $\theta_\infty = 6.0$.

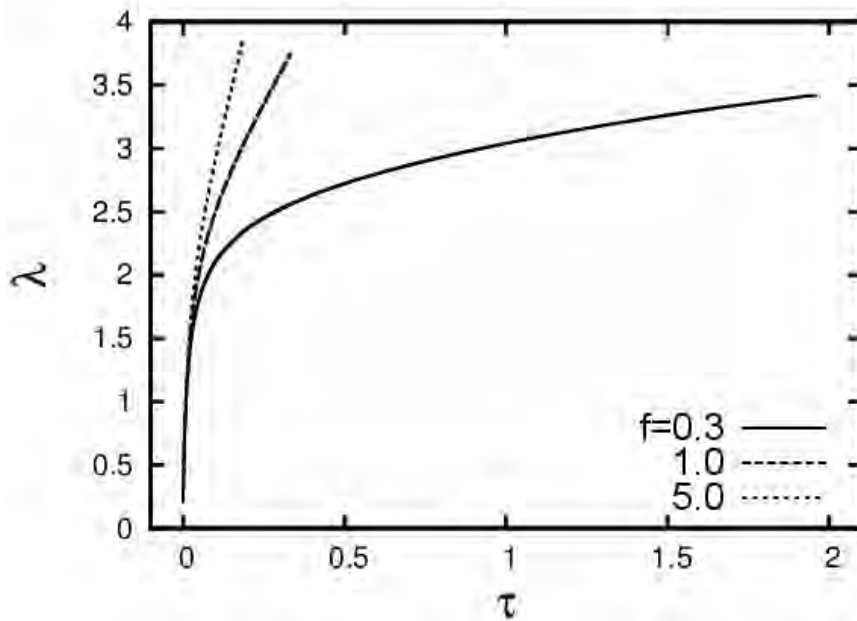


Figure 3.5 - Vaporization rate as a function of time for three different magnetic field frequencies $f = 0.3$ (a), 1.0 (b) and 5.0 (c) for $\theta_\infty = 6.0$.

the vaporization, which is responsible to decrease the temperature through mass loss. Under this ambient condition, the magnetic source $S(\theta, f)$, that depends on the local temperature, is able to increase the temperature of the thermal boundary

layer for values higher than that of the droplet surface. This increase of temperature in adjacent layers in the liquid side of the droplet surface is also evidenced in a previous work, where a semi-transparent droplet is internally heated by absorption of radiation from high temperature ambient atmosphere (TSENG; VISKANTA, 2006). In the present analysis, in addition to the gas phase heat flux, heat flux from the thermal boundary layer (Q^-) to the droplet surface raises the vaporization rates of ferrofluid droplet to above that described by classical models. In such models Q^- is always positive but in the present work Q^- can be negative too.

The droplet surface temperature θ_s and the vaporization rate λ as a functions of time are shown in Figs. (3.4) and (3.5). It is verified that both properties rise rapidly for high frequency conditions.

For low frequency conditions, the vaporization rate seems to approach a low variation regime, as shown in Fig. 3.5. For $f = 1.0$ and 5.0 , the vaporization rate and the temperature at the droplet surface increases almost at the same rate (Fig. 3.4). This feature is a consequence of the extra heat flux from the thermal boundary layer to the droplet surface.

3.3.2 Ambient atmosphere at boiling temperature

The following results show the ferrofluid droplet in a gaseous environment at the boiling temperature, $\theta_\infty = 1$. Temperature profiles in the thermal boundary layer are shown in Fig. 3.6 for magnetic field frequencies $f = 0.3, 1$ and 5 . Since in these cases the heat flux from the ambient atmosphere is low, the magnetic heat source controls almost integrally the heating process. In addition, because the magnetic nanoparticles distribution is uniform, the droplet has practically a uniform heating, resulting in a thermal boundary layer that presents only a small temperature variation. The droplet surface temperature presented in Fig. 3.7 follows a similar behavior to that described by the analytical solution (FACHINI; BAKUZIS, 2010), except for low magnetic field frequency at the end of the heating period. This indicates that the analytical solution is suitable for solving the problem in low ambient temperature condition.

Figure 3.8 shows the vaporization rate as a function of time. The results show a strong dependence of the vaporization rate on the magnetic field frequency. Unlike the surface temperature, the simulated and analytical values for the vaporization can not be compared directly. The comparison will be done indirectly through the fuel mass fraction at the droplet surface. Figure 3.9 shows the excellent agreement

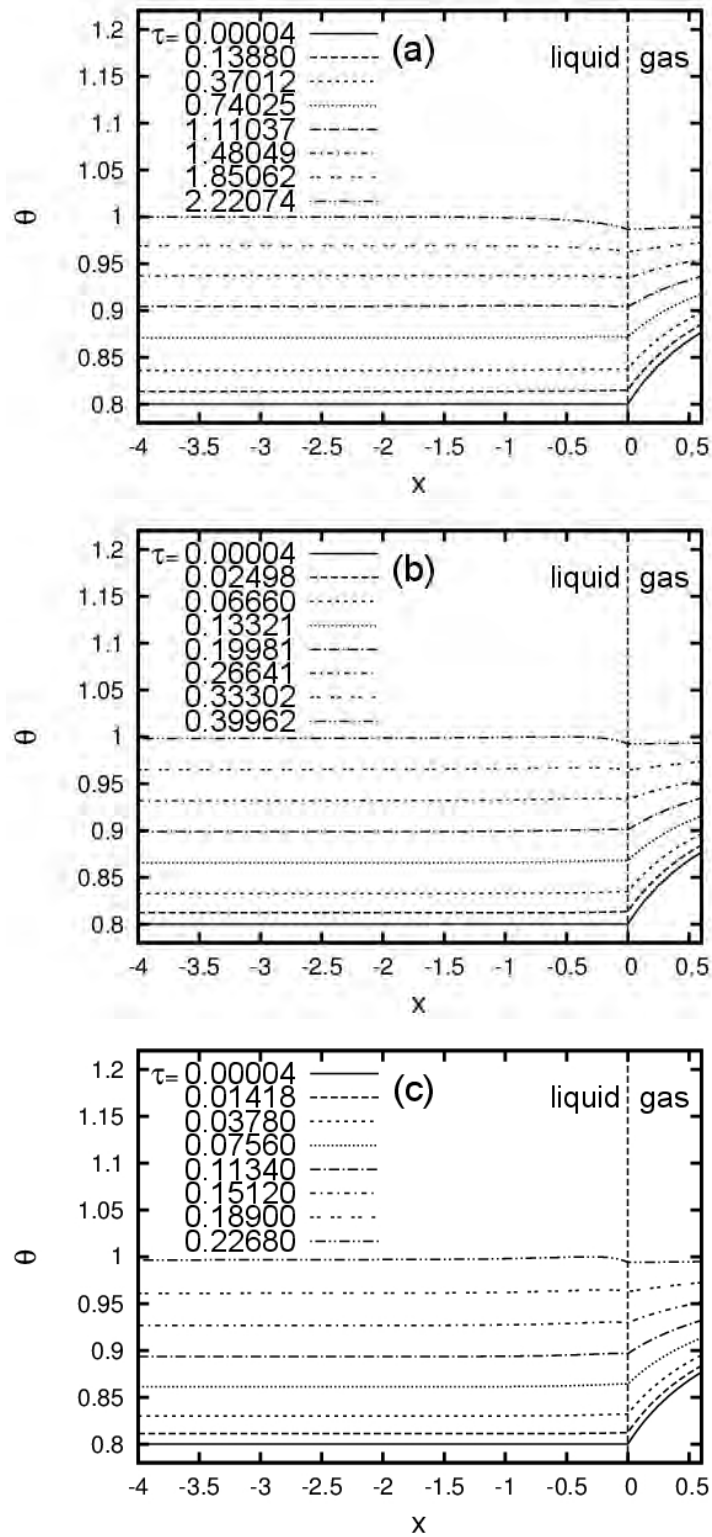


Figure 3.6 - Evolution of the temperature profile for three different magnetic field frequencies $f = 0.3$ (a), 1.0 (b) and 5.0 (c) for $\theta_\infty = 1.0$.

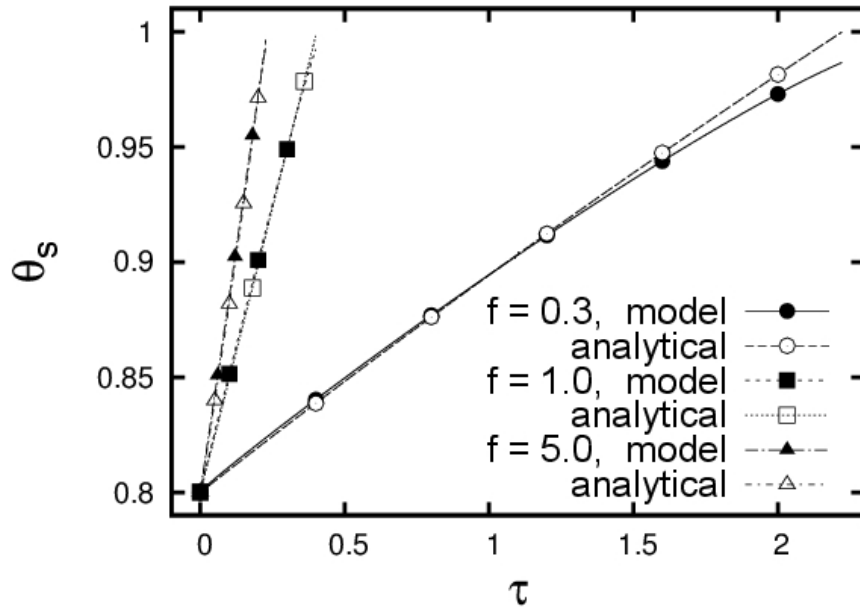


Figure 3.7 - Comparison of the results for the droplet surface temperature evolution from the present model and an analytical solution (FACHINI; BAKUZIS, 2010), for three different magnetic field frequencies $f = 0.3, 1.0, 5.0$ and ambient temperature $\theta_\infty = 1.0$.

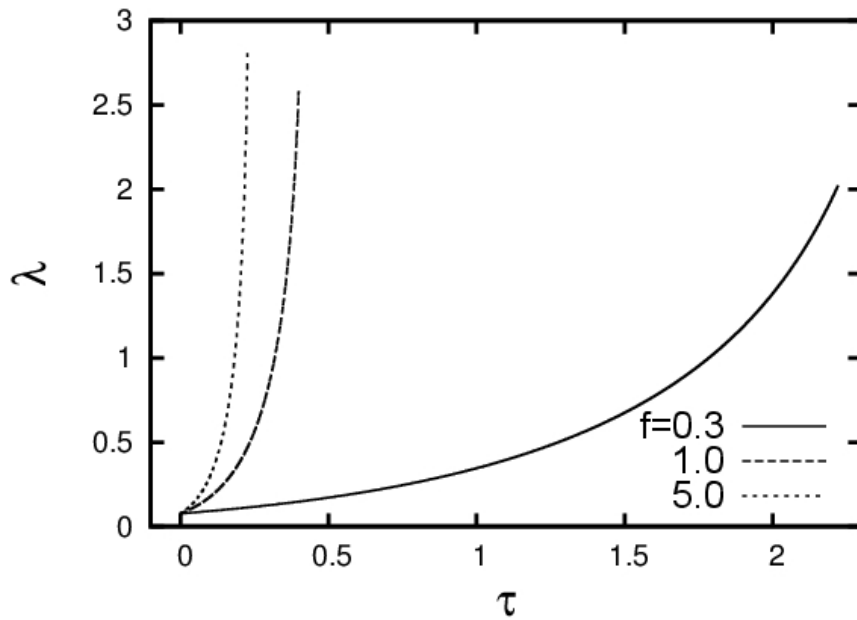


Figure 3.8 - Time evolution of the vaporization rate for three different magnetic field frequencies $f = 0.3, 1.0, 5.0$ and ambient temperature $\theta_\infty = 1.0$.

between the simulated and calculated values.

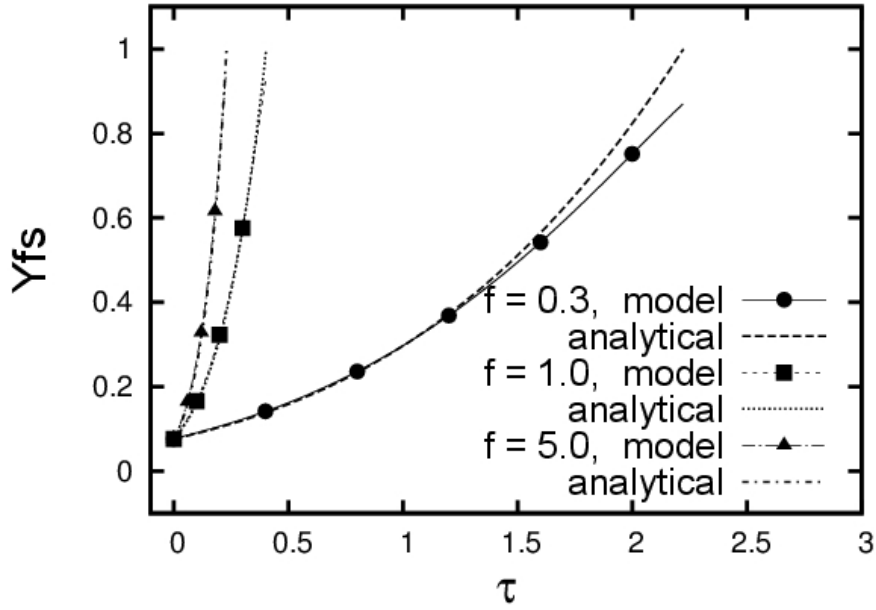


Figure 3.9 - Comparison of the results for the evolution of the fuel mass fraction at the droplet surface from the present model and an analytical solution (FACHINI; BAKUZIS, 2010), for three different magnetic field frequencies $f = 0.3, 1.0, 5.0$ and ambient temperature $\theta_\infty = 1.0$.

3.3.3 Low ambient atmosphere temperature

The droplet heating in an ambient atmosphere with a lower temperature than the initial droplet temperature is analyzed, specifically the case $\theta_\infty = 0.75$ is considered. The temperature profiles are shown in Fig. 3.10 for different values of magnetic field frequency.

The results are similar to the previous case ($\theta_\infty = 1$), but the thermal boundary layer cannot be observed easily. Furthermore the heating time is practically the same as that for the ambient temperature $\theta_\infty = 1$, as shown in Fig. 3.6. As this happens at low ambient temperature as well as at $\theta_\infty = 1$, the droplet heating depends practically only on the magnetic source. Hence, the heating time is controlled just by the magnetic field frequency.

The small influence of the ambient temperature on the heating process can be quantified evaluating the heat flux across the droplet surface, which is given by $q^- = Q^- / (AP_m)^{1/2} = a^2 (\partial\theta / \partial x)_{x=a^-}$. The value $q^- < 0$ represents a heat loss from the droplet to the ambient atmosphere, whereas $q^- > 0$ represents heat gain from gas phase. Figure 3.11 shows the heat flux across the droplet surface as a function

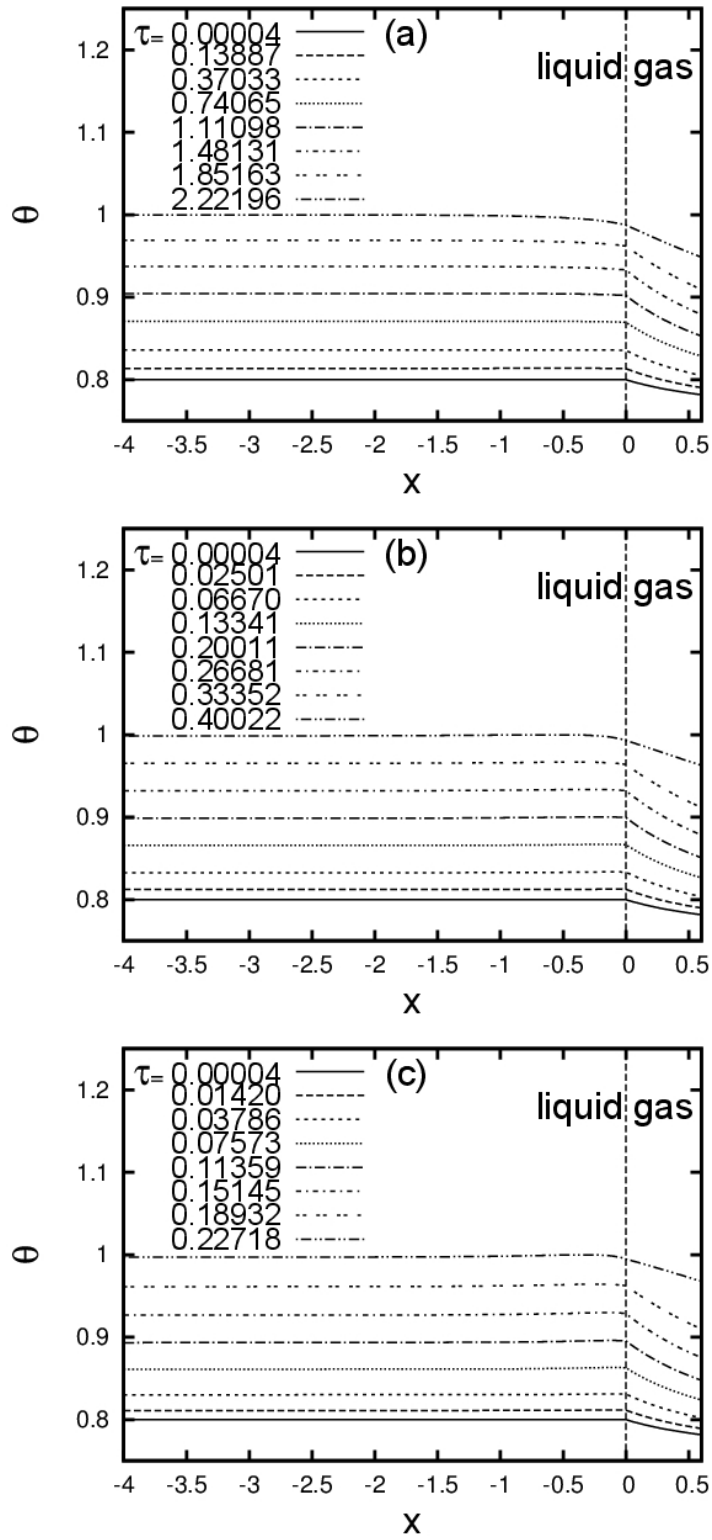


Figure 3.10 - Evolution of the temperature profile for three different magnetic field frequencies $f = 0.3$ (a), 1.0 (b) and 5.0 (c) and $\theta_\infty = 0.75$.

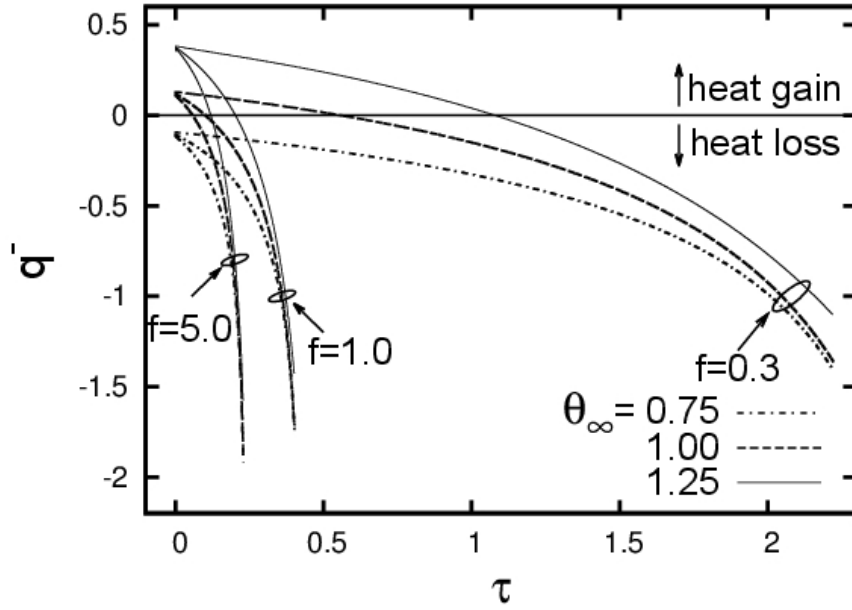


Figure 3.11 - Heat flux across the droplet surface as a function of time for different magnetic field frequencies $f = 0.3, 1.0, 5.0$ under the conditions $\theta_\infty = 0.75, 1.0, 1.25$. ($q^- < 0$ represents heat loss from the droplet to the ambient atmosphere and $q^- > 0$ represents heat gain from the gas phase).

of time for different conditions of the ambient temperature and the magnetic field frequency. For conditions where the ambient temperature is higher than the initial temperature of the droplet, the droplet initially receives heat from the ambient ($q^- > 0$). As the vaporization rate increases, vaporization heat loss leads to smaller values for the droplet surface temperature compared with that of the core ($q^- < 0$), as shown in Fig 3.11. On the contrary, in the case where the ambient temperature is lower than the initial temperature of the droplet, the droplet loses heat to the ambient during the whole heating period. The results reinforce the fact that the frequency f controls the heating and vaporization of the droplet in low temperature atmosphere.

3.3.4 Low ambient atmosphere temperature with $Y_\infty = 0.2$

Until now the vapor mass fraction in the ambient atmosphere was assumed to be zero. In this section, results for a ferrofluid droplet in an ambient atmosphere with temperature $\theta_\infty = 0.75$ and fuel mass fraction $Y_\infty = 0.2$ are presented. As gas phase is at a low temperature and the vapor mass fraction at the droplet surface satisfies the condition $Y_s < 0.2$, then the vapor near the droplet surface is condensed in the initial period of the heating process. In this work, the hypotheses that the

condensed vapor on the droplet surface mixes instantaneously with the ferrofluid and the magnetic nanoparticles distribution does not change significantly are assumed. Without this consideration, the droplet would have a liquid layer on its surface with absence of nanoparticles. This feature is not covered by the present model.

It is known that, the surface of the droplet is heated during the condensation, but the temperature increment is insignificant compared with that imposed by the magnetic source. More precisely, for the condition $f = 0.3$, the droplet surface presents an increase in temperature of the order of 10^{-5} in relation to the initial temperature inside of the droplet. Figure 3.12 shows the droplet radius as a function of time, from which an increase in the radius during condensation process is observed. Finally, Figure 3.13 shows the vaporization rate as a function of time. Negative values for the vaporization rate represents the condensation process. During the condensation,

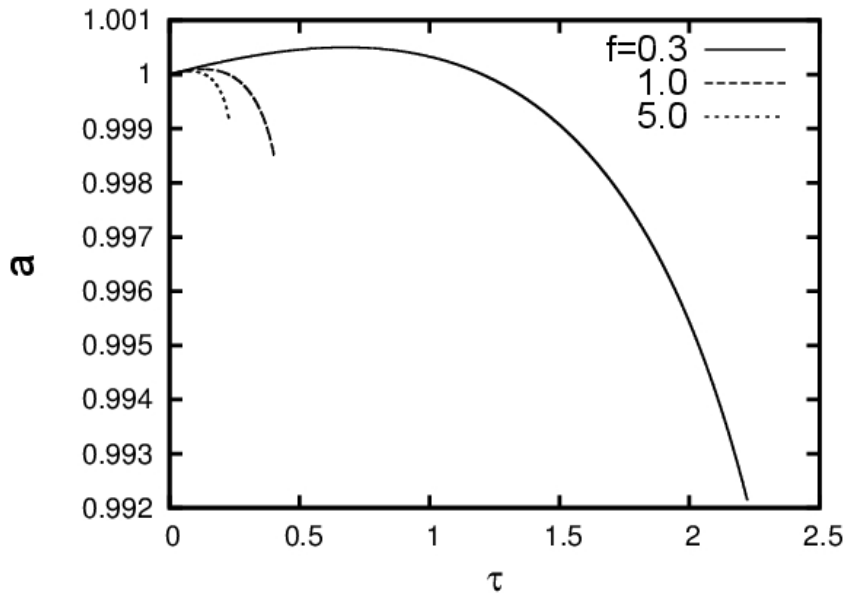


Figure 3.12 - Time evolution for the square droplet radius for three different magnetic field frequencies $f = 0.3, 1.0, 5.0$, ambient temperature $\theta_\infty = 0.75$ and ambient fuel mass fraction $Y_\infty = 0.2$

the mass flux of the vapor controls the droplet surface temperature and after that the magnetic source is responsible for increasing the droplet surface temperature. The behavior shown in Fig. 3.13 is similar to that presented in Fig. 3.8.

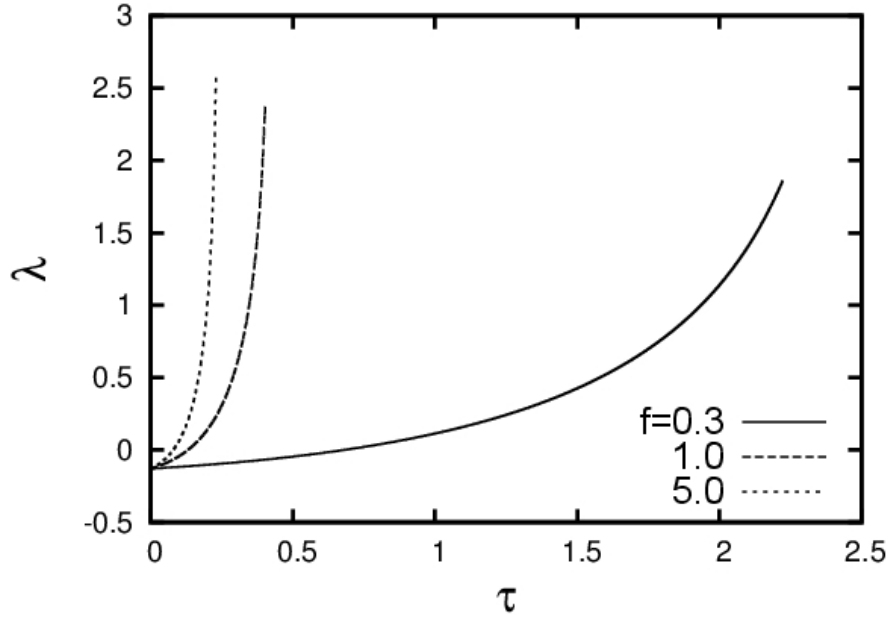


Figure 3.13 - Time evolution for the vaporization rate for three different magnetic field frequencies $f = 0.3, 1.0, 5.0$, ambient temperature $\theta_\infty = 0.75$ and ambient fuel mass fraction $Y_\infty = 0.2$

3.3.5 Influence of the Lewis number

The hypothesis of Lewis number equal to unity was considered to simulate the above cases, which is appropriate to some applications. The following results show the effect of Lewis number Le on temperature profiles in the thermal boundary layer. Figure 3.14 show the temperature profiles during the ferrofluid droplet heating at high ambient temperature, $\theta = 6.0$, and high magnetic field frequency, $f = 5.0$, for $Le = 0.5, 1.0$ and 1.8 . The results show that the Lewis number has a direct influence on the thermal boundary layer thickness and on the temperature profile. Since Lewis number measures the thermal diffusivity in relation to the mass diffusivity, then the vaporization rate, which depends on the gas phase mass diffusivity, increases as the Lewis number decreases. Consequently, due to the increase of the heat loss by the vaporization, the droplet surface temperature decreases. With the increasing temperature inside the thermal boundary layer and the decreasing droplet surface temperature, the heat transfer from the thermal boundary layer to the droplet surface increases by decreasing the vapor Lewis number, as seen in Fig. 3.14. This extra heat flux to the droplet surface augments the vaporization rate.

Figure 3.15 shows the thickness of the thermal boundary layer as a function of time for $Le = 0.5, 1.0$ and 1.8 . When the condition favors the augment of the droplet

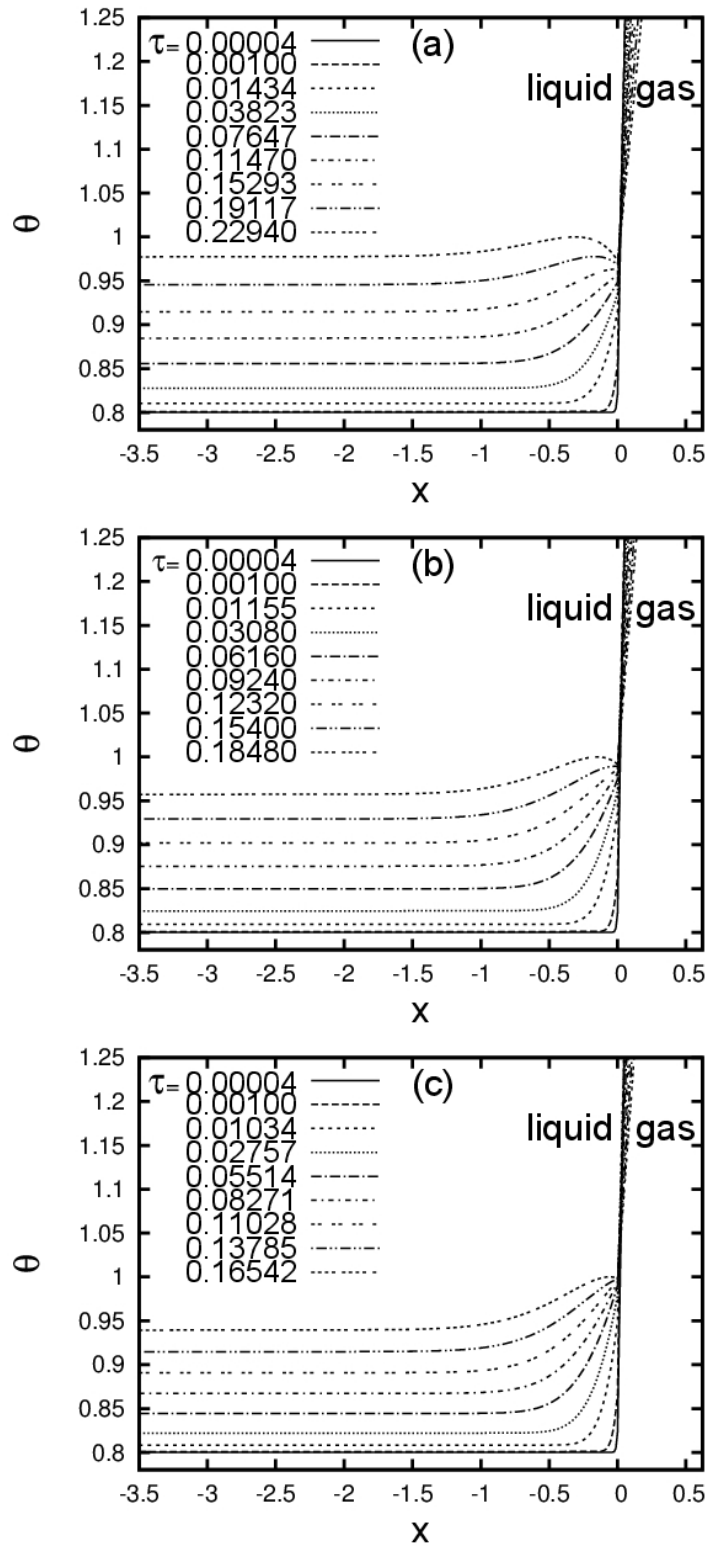


Figure 3.14 - Time evolution of the temperature profile for three different values of the Lewis number $Le = 0.5$ (a), 1.0 (b) and 1.8 (c), magnetic field frequency $f = 5.0$ and ambient temperature $\theta_\infty = 6.0$.

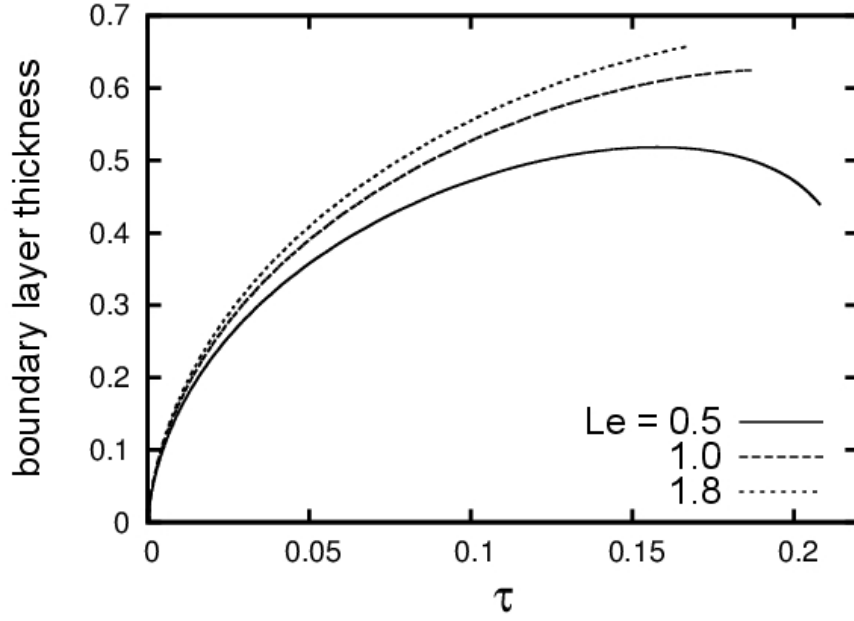


Figure 3.15 - Time evolution of the boundary layer thickness for three different Lewis number $Le = 0.5, 1.0$ and 1.8 , magnetic field frequency $f = 5.0$ and ambient temperature $\theta_\infty = 6.0$.

surface temperature θ_s ($Le > 1$), the difference between θ_s and the droplet core temperature increases and, as a result, the thickness of the thermal boundary layer augments. In addition, since the heat loss by vaporization decreases the difference between the surface temperature and the droplet core temperature, the thickness thermal boundary layer decreases for $Le < 1$.

Figures 3.16 and 3.17 show the vaporization rate and the droplet surface temperature, respectively, as functions of time for different values of Lewis number. Since the fuel mass diffusivity controls the droplet vaporization, the vaporization rate is larger for smaller values of the Lewis number, as shown in Fig. 3.16. However, the increase of the vaporization rate causes an increase on the droplet heat loss and a decrease on the droplet surface temperature, as seen in Fig. 3.17. Consequently, the intensity of the magnetic source is different inside the thermal boundary layer, leading to a local maximum on the temperature profile.

3.4 Comparison of magnetic and laser heating

In this section, the magneto relaxation heating of ferrofluid droplet (water-maghemite) is compared with the heating of pure water droplet irradiated by an unpolarizer plane wave CO_2 laser beam (ARMSTRONG, 1984; ARMSTRONG et al.,

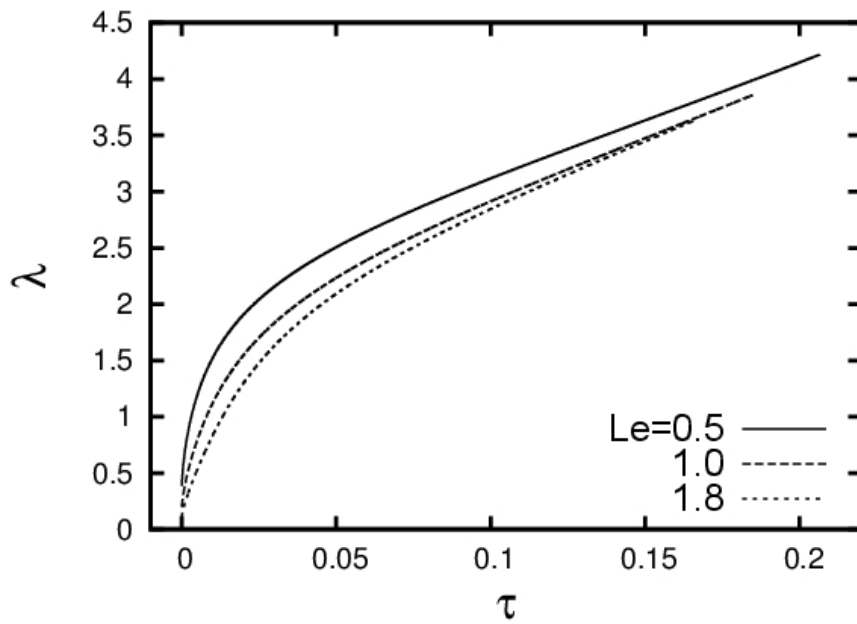


Figure 3.16 - Time evolution of the vaporization rate for three different Lewis number $Le = 0.5, 1.0$ and 1.8 , magnetic field frequency $f = 5.0$ and ambient temperature $\theta_\infty = 6.0$.

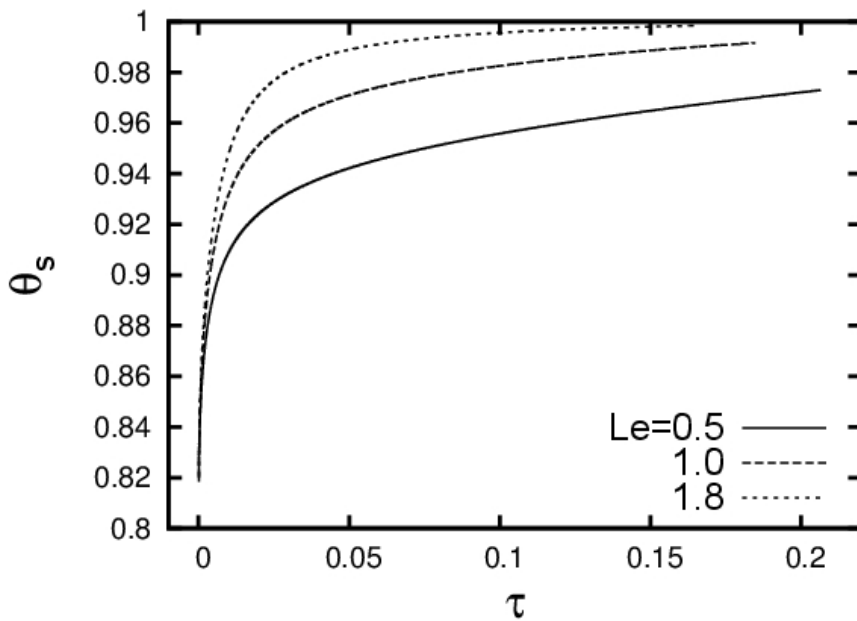


Figure 3.17 - Time evolution of the droplet surface temperature for three different Lewis number $Le = 0.5, 1.0$ and 1.8 , magnetic field frequency $f = 5.0$ and ambient temperature $\theta_\infty = 6.0$.

1986; PARK; ARMSTRONG, 1989). The case analyzed in laser heating considers a

droplet of radius $a = 10 \mu m$, laser power, of $I_L = 10^6 W/cm^2$ and complete absorption of laser beam by the droplet. The droplet with initial temperature of $25 \text{ }^\circ C$ is heated up to $305 \text{ }^\circ C$ that is a value somewhat smaller than the superheat limit $T_{su} = 0.9T_{cr}$ (T_{cr} is the critical temperature and equal to $373.85 \text{ }^\circ C$). These conditions are assigned for the case of the rapid heating of irradiated aerosols (PARK; ARMSTRONG, 1989). Therefore, to compare magneto relaxation and laser heating, the former process will be permitted running up to the droplet core temperature to achieve $T = 305^\circ C$.

The comparison between the two heating methods is performed by comparing the results for P_m and the dimensionless laser heat source P_L (PARK; ARMSTRONG, 1989), which is defined following the procedure adopted for the magnetic one,

$$P_L = \frac{4\pi Re(n)Im(n)S_L I_L / \lambda_{lw}}{\rho_l c_l T_b / t_c^*} \quad (3.21)$$

in which $n = 1.179 - i0.071$, $S_L = |E|^2 / |E_{inc}|^2$ (E is the electric field at a point and E_{inc} is the electric field of incident laser beam) and λ_{lw} is the laser wavelength. The conditions addressed in the fast heating regime with $S_L = 1$ leads to $P_L = 3760$. The simulations point out a heating time about $1.41 \mu m$ (PARK; ARMSTRONG, 1989). The simulations for magneto relaxation heating show the same heating time for $P_m = 1950$ and magnetic field frequency $f = 4$. This result indicates that magneto relaxation is able to heat up a larger droplet (about $a = 300 \mu m$) in the same time with 52% of source power. The comparison between the two simulations is exhibited in Fig. 3.18.

Not only the difference on the parameter values is observed but also the behavior of the temperature profile close to the droplet surface. In the present model the term $(AP_m)^{1/2} \gg 1$, in the energy conservation condition at the droplet surface Eq. (3.9), demands a heat flux at the droplet surface in the liquid phase of order $(AP_m)^{-1/2} \ll 1$ to have order unity for that heat flux. The condition leads to a very small difference of temperature between the droplet surface and the droplet interior, explaining the small variation of temperature even close to the surface. In the case of laser heating, the temperature profile changes significantly close to the droplet surface and the reason for that is different vaporization model adopted, which imposes a large vaporization rate resulting in low droplet surface temperature.

Since the laser source is considered constant in this case, the temperature variation with time is also constant. However, since the magnetic source depends on the tem-

perature for high frequencies, the temperature evolution changes with time, as seen in Fig. 3.18.

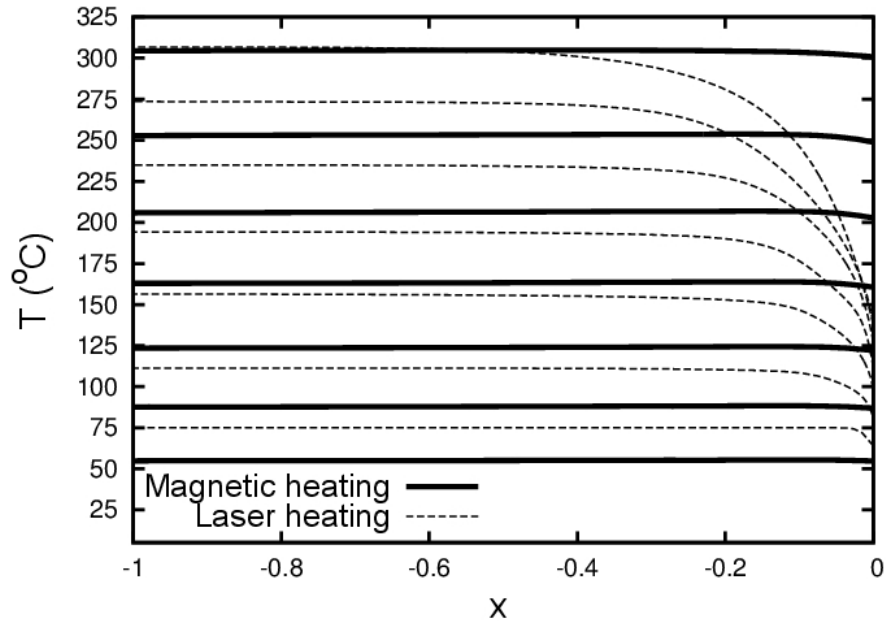


Figure 3.18 - Temperature profiles for magnetic relaxation heating ($P_m = 1950$ and $f = 4$) and irradiated laser heating model (PARK; ARMSTRONG, 1989) at times, $t = 0.2, 0.4, 0.6, 0.8, 1.0, 1.2, 1.4 \mu s$.

4 COMBUSTION PROBLEM

The hypothesis that the reaction is rapid, implies that the reaction zone is thin and very little reactants can leak through the flame. The heat generated by the flame is transported both outward to the ambient atmosphere and inward to droplet, which heats and simultaneously vaporizes it. Similar to the vaporization case without combustion, for a pure fuel, much of droplet heating is rapidly over and the droplet surface area then regresses at a constant rate. At this point it is appropriate to recognize the similarity between droplet vaporization and droplet combustion. Apart from the gas-phase reactions, the detailed transport mechanisms within the droplet and the vaporization process at its surface are qualitatively the same in both cases. Thus, during combustion, the droplet simply perceives the flame as a hotter “ambient” located at a somewhat closer distance (LAW, 1982; SIRIGNANO, 1983).

4.1 Model formulation

The model considers a spherical ferrofluid fuel droplet burning in a quiescent oxidizing atmosphere. All processes, both in the liquid and the gas phase are spherically symmetrical, and the problem can be treated as one-dimensional in the radial direction. The problem is solved in both liquid and gas phases and the appropriate matching condition at the droplet surface is satisfied. In the liquid phase, the following properties are constant: density ρ_l^* , specific heat c_l^* and thermal conductivity k_l^* . In the gas phase, far away from the droplet, the properties density ρ_∞^* , temperature T_∞^* , specific heat at constant pressure c_p^* and thermal conductivity k_∞^* are constant. The conservation equations for both liquid and gas phases are written using the following dimensionless variables:

$$t \equiv \frac{t^*}{t_c^*}, \quad r \equiv \frac{r^*}{a^*(0)}, \quad \theta \equiv \frac{T^*}{T_b^*}, \quad \rho \equiv \frac{\rho^*}{\rho_\infty^*},$$

$$u \equiv \frac{u^* a^*(0)}{\alpha_\infty^*}, \quad Y_O \equiv \frac{Y_O^*}{Y_{O_\infty}^*}, \quad Y_F \equiv Y_F^* \quad a \equiv \frac{a^*}{a^*(0)},$$

in which the time t^* is scaled by the order of magnitude of the droplet life time $t_c^* \equiv (a^*(0))^2 / (\alpha_\infty^* \varepsilon)$, with $\varepsilon \equiv \rho_\infty^* / \rho_l^* \ll 1$ and $\alpha_\infty^* \equiv k_\infty^* / (c_p^* \rho_\infty^*)$ being the thermal diffusivity. The radial coordinate r^* is scaled by the initial droplet radius $a^*(0)$, and temperature T^* by the boiling temperature T_b^* . The dimensionless variables θ , ρ , v , Y_O , Y_F and a are: temperature, gas density, gas velocity, oxidant mass fraction, fuel mass fraction and instantaneous droplet radius, respectively. Superscript $*$ represents variables in dimensional form and subscript b stands for boiling condition. The species mass fractions Y_F^* and Y_O^* are intrinsically dimensionless, however they

are written above as dimensional variables, $()^*$, to follow a consistent nomenclature and to allow the definition of the normalized variable Y_O .

The pressure condition considered in this analysis lead to the thermal inertia of the liquid to be much larger than that of the gas, hence $\varepsilon \equiv \rho_\infty/\rho_l \ll 1$ (WALDMAN, 1975). Under such a condition, the gas phase is in quasi-steady state, which simplifies the solution of the droplet combustion problem. Therefore the results do not apply to diesel and rocket engines operational conditions.

The dimensionless conservation equations for mass and energy of the liquid phase (droplet) are (FACHINI; BAKUZIS, 2010)

$$\frac{da^2}{dt} = -3\lambda, \quad (4.1)$$

$$\frac{\partial\theta}{\partial t} - \frac{A}{r^2} \frac{\partial}{\partial r} \left(r^2 \frac{\partial\theta}{\partial r} \right) = P_m \frac{f^2 t_m(\theta)}{1 + (f t_m(\theta))^2}, \quad (4.2)$$

in which $\lambda \equiv \dot{m}(t^*)c_p^*/(4\pi k_\infty^* a_0^*)$ is the dimensionless vaporization rate, $\dot{m}(t^*)$ is the dimensional vaporization rate which is a function of time and the parameter A is defined as $c_p^*k_l^*/(c_l^*k_g^*)$. The right-hand side of Eq. (4.2) represents the magnetic heat source, Eq. (2.13), in dimensionless form, in which the parameter

$$P_m = \frac{\mu_0^* \chi_0^* (H_0^*)^2 / 2}{\rho_l^* c_l^* T_b^*} \frac{t_c^*}{t_{mb}^*} \quad (4.3)$$

represents the ratio of the magnetic source power to the thermal source power. The analysis considers the case where $P_m \gg 1$. As mentioned above, the effective relaxation time t_m ($\equiv t_m^*/t_{mb}^*$) is equal to the Brownian relaxation time $t_m = t_B$, while the dimensionless frequency is defined as $f \equiv 2\pi f^* t_{mb}^*$. The Brownian relaxation time at the boiling temperature is denoted by $t_{mb}^* = t_{Bb}^*$. The heat transfer model described by Eq. (4.2) results in a boundary layer model because of the assumption that $P_m \gg 1$.

As already mentioned, the current analysis is based upon the two assumptions regarding the ferrofluid: a) that the magnetic nanoparticles distribution inside the droplet is uniform and b) that the magnetic source power is much larger than the thermal source power provided by heat transfer from the gas phase ($P_m \gg 1$). The first assumption leads to uniform heating of the droplet core, while the second leads to a thermal boundary layer adjacent to the droplet surface in the liquid side, as will be shown next.

For $P_m \gg 1$, in the core, heat conduction can be neglected compared to the magnetic source term in Eq. (4.2). As a result, the temperature profile is only time dependent for $t = O(P_m^{-1})$ in the droplet core (FACHINI; BAKUZIS, 2010). However that solution to Eq. (4.2) cannot be matched to the temperature profile in the gas phase resulting from the heat flux from the flame into the droplet. Matching the time dependent temperature profile in the core to the quasi-steady temperature profile in the gas phase requires accounting for the thermal boundary layer that appears in the liquid, close to the droplet surface. In this context, the aim of this work is thus to analyze the droplet combustion problem using the thermal boundary layer model.

In the thermal boundary layer formulation, the time variable t needs rescaling according to $\tau = P_m t$ and the spatial variable r in the liquid phase is replaced by x , defined by $r = a + \delta x$, with $\delta \ll 1$, specifically, $\delta \equiv (A/P_m)^{1/2}$. Furthermore, the thermal boundary layer model is valid as long as the condition $\delta \ll a(t)$ is satisfied. Thus, when the droplet lifetime reaches its end, when $\delta \sim a(t)$, the boundary layer assumption will no longer be valid, but Eq. (4.2), using the r coordinate will then describe the evolution in time and space of the temperature profile.

When using the variables τ and x , all terms in Eq. (4.2) become of the same order of magnitude. As already mentioned, magnetic heating is taken as due to the Brownian mechanism, whose relaxation time is reciprocal to temperature $\tau_m(\theta) = 1/\theta$ (FACHINI; BAKUZIS, 2010; MAENOSONO; SAITA, 2006). Therefore, using rescaled time and space, Eqs. (4.1) and (4.2) are written as

$$\frac{d(a)^3}{d\tau} = -3 \frac{\lambda}{P_m}, \quad (4.4)$$

$$\frac{\partial \theta}{\partial \tau} + \frac{1}{\delta} \frac{da}{d\tau} \frac{\partial \theta}{\partial x} - \frac{\partial^2 \theta}{\partial x^2} = \frac{f^2 \theta}{\theta^2 + f^2}. \quad (4.5)$$

The convective term proportional to da/dt in Eq. (4.5) can be neglected because it is of order $P_m^{-1/2}$, as was shown in the previous chapter.

In the present chapter a simplified kinetic mechanism is considered, irreversible one step reaction between a fuel F , oxidant O yielding a product P ,



in which ν represents the amount of oxidant required to burn the unit mass fuel to yield a mass $1 + \nu$ of products with a heat release Q per unit mass of fuel.

The conservation equations for the gas phase are (FACHINI, 1999; FACHINI; LINÁN, 1999):

$$\varepsilon P_m \frac{\partial \rho}{\partial \tau} + \frac{1}{r^2} \frac{\partial}{\partial r} (r^2 \rho v) = 0, \quad (4.7)$$

$$\varepsilon P_m \rho \frac{\partial Y_i}{\partial \tau} + \rho u \frac{\partial Y_i}{\partial r} - \frac{1}{r^2} \frac{\partial}{\partial r} \left(\frac{r^2 \theta^n}{Le_i} \frac{\partial Y_i}{\partial r} \right) = -s_i \omega_F, \quad i = O, F, \quad (4.8)$$

$$\varepsilon P_m \rho \frac{\partial \theta}{\partial \tau} + \rho u \frac{\partial \theta}{\partial r} - \frac{1}{r^2} \frac{\partial}{\partial r} \left(r^2 \theta^n \frac{\partial \theta}{\partial r} \right) = Q \omega_F, \quad (4.9)$$

in which $s_F = 1$, $s_O \equiv \nu/Y_{O\infty}^*$, ω_F is the fuel consumption rate, $Q \equiv Q^*/(c_p T_\infty^*)$ is the dimensionless heat of combustion and Y_i and Le_i represent the mass fraction and Lewis number of species i , respectively. Recalling, $\varepsilon \equiv \rho_\infty^*/\rho_l^* \ll 1$.

This study focuses upon a very short droplet heating time, because of the assumption $P_m \gg 1$. However, the characteristic time scale τ is not short enough to capture transient transport in the gas phase. In effect, even though $P_m \gg 1$, $\varepsilon \ll 1$ and the product is taken to satisfy the condition $P_m \varepsilon \ll 1$. Under that condition, the transport phenomena in the gas phase remain quasi-steady. The mass conservation equation is then described by $r^2 \rho u = \lambda(\tau)$ and the species and energy conservation equations, by

$$\frac{\lambda}{r^2} \frac{\partial Y_i}{\partial r} - \frac{1}{r^2} \frac{\partial}{\partial r} \left(\frac{r^2 \theta^n}{Le_i} \frac{\partial Y_i}{\partial r} \right) = s_i \omega_F, \quad i = O, F, \quad (4.10)$$

$$\frac{\lambda}{r^2} \frac{\partial \theta}{\partial r} - \frac{1}{r^2} \frac{\partial}{\partial r} \left(r^2 \theta^n \frac{\partial \theta}{\partial r} \right) = Q \omega_F. \quad (4.11)$$

The solution to Eqs. (4.4), (4.5), (4.10) and (4.11) requires that the temperature profile inside the droplet satisfies the following conditions: in the droplet core

$$\left(\frac{\partial \theta}{\partial x} \right)_{x \rightarrow \infty} \rightarrow 0, \quad (4.12)$$

while at the droplet surface ($r = a$),

$$\left(r^2 \theta^n \frac{\partial \theta}{\partial r} \right)_{r=a^+} = \lambda L - a^2 (A.P_m)^{1/2} \left(\frac{\partial \theta}{\partial x} \right)_{x=0^-} = \lambda L_{eff}, \quad (4.13)$$

$$- \left(\frac{r^2 \theta^n}{Le_F} \frac{\partial Y_F}{\partial r} \right)_{r=a^+} = \lambda (1 - Y_{Fs}), \quad (4.14)$$

at the flame

$$\theta - \theta_f = Y_F = Y_O = 0 \quad \text{at} \quad r = r_f, \quad (4.15)$$

and finally, in the ambient atmosphere

$$\theta - \theta_\infty = Y_F = Y_O - 1 = 0 \quad \text{in} \quad r \rightarrow \infty, \quad (4.16)$$

L ($\equiv L^*/(c_p T_\infty)$) represents the dimensionless vaporization latent heat. According to Eq. (4.13), L_{eff} is the effective latent heat of vaporization; $x = 0^-$ stands for the liquid-side phase and $r = a^+$ stands for the gas-side phase.

Whereas the chemical time is much shorter than the residence time (very large values of the Damköhler number) in a first approximation, the reactants are assumed not to coexist. Thus the oxygen and fuel domains are separated by a negligible thickness structure (a flame sheet) for infinitely fast chemical reaction. These hypotheses allow for using the Shvab-Zel'dovich-Liñán formulation (no-unity Lewis number Shvab-Zel'dovich formulation) (LINÁN, 1991; LINÁN, 2001) to eliminate the chemical reaction term in Eqs. (4.10) and (4.11). This yields

$$\frac{\lambda}{r^2} \frac{\partial \bar{H}}{\partial r} - \frac{1}{r^2} \frac{\partial}{\partial r} \left(r^2 \theta^n \frac{\partial \bar{H}}{\partial r} \right) + N(\bar{Z}) \frac{\lambda}{r^2} \frac{\partial \bar{Z}}{\partial r} = 0 \quad (4.17)$$

$$Le(\bar{Z}) \frac{\lambda}{r^2} \frac{\partial \bar{Z}}{\partial r} - \frac{1}{r^2} \frac{\partial}{\partial r} \left(r^2 \theta^n \frac{\partial \bar{Z}}{\partial r} \right) = 0 \quad (4.18)$$

in which $\bar{H} = (s + 1)Le_F \theta / Q + Y_O + Y_F$, $\bar{Z} = sY_F - Y_O + 1$, $s = s_O Le_O / Le_F$,

$$Le(\bar{Z}) = \begin{cases} Le_F, & \bar{Z} > 1 \\ Le_O, & \bar{Z} < 1 \end{cases} \quad \text{and} \\ N(\bar{Z}) = \begin{cases} (Le_F - 1)/s, & \bar{Z} > 1 \\ (1 - Le_O), & \bar{Z} < 1 \end{cases} .$$

The boundary conditions for Eqs. (4.17) and (4.18) are: at the droplet surface ($r = a$)

$$\bar{H}(a) = \frac{(s + 1)Le_F \theta_s}{Q} + Y_{Fs}, \quad (4.19)$$

$$\bar{Z}(a) = sY_{Fs} + 1, \quad (4.20)$$

$$\left(r^2 \theta^n \frac{\partial \bar{H}}{\partial r} \right)_{r=a} = \frac{\lambda(s + 1)Le_F Le_{eff}}{Q} - \lambda Le_F (1 - Y_{Fs}), \quad (4.21)$$

$$\left(r^2 \theta^n \frac{\partial \bar{Z}}{\partial r} \right)_{r=a} = -\lambda Le_F s (1 - Y_{Fs}), \quad (4.22)$$

at the flame ($r = r_f$)

$$\bar{H}(r_f) = \frac{(s+1)L_{eF}\theta_f}{Q} \quad (4.23)$$

$$\bar{Z}(r_f) = 1 \quad (4.24)$$

and in the ambient atmosphere ($r \rightarrow \infty$)

$$\bar{H}(r \rightarrow \infty) = \frac{(s+1)L_{eF}}{Q} + 1 \quad (4.25)$$

$$\bar{Z}(r \rightarrow \infty) = 0 \quad (4.26)$$

As a result, the system of Eqs. (4.17) to (4.26) can be solved analytically. The solution is exhibited elsewhere (FACHINI, 1999; FACHINI; LINÁN, 1999). The effective latent heat of vaporization L_{eff} , the flame position r_f , the flame temperature θ_f and the fuel mass fraction at the droplet Y_{Fs} can be expressed as a function of the droplet surface temperature θ_s , which is determined by integration of Eqs. (4.4) and (4.5) (FACHINI, 1999). Thus, the effective heat of vaporization is given by

$$L_{eff} = \frac{Q + (1 - \theta_s - Q) [s/(s+1)]^{1/LeO}}{(1 - Y_{Fs})^{-1/LeF} - [s/(s+1)]^{1/LeO}}, \quad (4.27)$$

Since vapor and liquid are assumed to be in equilibrium at the interface, the Clausius-Clapeyron relation, $Y_{Fs} = \exp[\gamma(1 - \theta_b/\theta_s)]$, can be used to relate the fuel mass fraction Y_{Fs} and the droplet surface temperature θ_s , in which $\gamma \equiv L^*/(R_g T_b^*)$; R_g is the gas constant and T_b^* is the dimensional boiling temperature.

Also, the vaporization function $\beta \equiv \lambda/a$, which is a constant in the classical model, is obtained:

$$\beta = \int_{\theta_s}^{\theta_f} \frac{r^n}{r - \theta_s + L_{eff}} dr + \int_{\theta_f}^{\theta_\infty} \frac{r^n}{r - Q - \theta_s + L_{eff}} dr, \quad (4.28)$$

the flame position is given by

$$r_f/a = 1 + \left(\int_{\theta_s}^{\theta_f} \frac{r^n}{r - \theta_s + L_{eff}} dr \right) / \left(\int_{\theta_f}^{\theta_\infty} \frac{r^n}{r - Q - \theta_s + L_{eff}} dr \right), \quad (4.29)$$

and the flame temperature is determined as

$$\theta_f = \theta_\infty + (Q + \theta_s - \theta_\infty - L_{eff}) \left[1 - \left(\frac{s}{s+1} \right)^{1/LeO} \right]. \quad (4.30)$$

4.1.1 Numerical strategy

Once the gas phase problem is solved, the solution for Eqs. (4.4) and (4.5) is obtained numerically, satisfying the boundary condition at the droplet interface, Eq. (4.13), and the temperature profile in the droplet core, Eq. (4.12). The strategy for solving the problem is to search iteratively for a value of the droplet surface temperature θ_s that satisfies both the gas and liquid phase problems, Eqs. (4.4) to (4.12), under matching conditions, Eqs. (4.13) and (4.14).

To validate the numerical code the case where $f \ll 1$ is used. Then the source term in Eq. (4.5) becomes negligible because of its dependence on f^2 ; the external magnetic field does not transfer energy to the liquid. Thus, Eq. (4.5) with no magnetic effect can be solved analytically:

$$\theta(\tau, x) = \theta(0) + (\theta_s - \theta(0))[1 - \text{erf}(x/\tau^{1/2})], \quad (4.31)$$

in which $\theta(0)$ is the initial droplet temperature. Therefore, the heat flux at the droplet surface in the liquid side, $\partial\theta/\partial x|_{x=0^-}$, is obtained analytically as a function of the droplet temperature θ_s and time τ . Thus, the boundary condition at the droplet surface, Eq. (4.13), is satisfied for a given temperature θ_s at each instant of time. Recalling that λ and L_{eff} are functions of θ_s . For validation purposes, the evolution of the droplet temperature for $f \ll 1$ obtained numerically is compared with the analytical solution. The comparison is shown in Fig. 4.1. The showing that the numerical results for $f \ll 1$ are in agreement with the analytical results for $f = 0$.

4.2 Results

The results obtained for heating, vaporization and burning of a ferrofluid fuel droplet (radius $a = 70 \mu m$) under the influence of an alternating magnetic field are presented and discussed in this section. The base fuel is n-heptane at initial temperature $\theta(0) = 0.8$ (which corresponds to 298 K). The properties of the n-heptane are: density $684 \times 10^3 \text{ g/m}^3$, viscosity $3.8610^{-4} \text{ N s/m}^2$, thermal conductivity 0.6 J/(m s K) and specific heat 2.2359 J/(g K) . The properties of the ambient atmosphere (air) in a region far from the droplet at 298 K are: density 1100 g/m^3 , thermal conductivity 0.025 J/(m s K) , specific heat 1.0 J/(g K) and oxidant mass fraction $Y_{O_\infty}^* = 0.23$. For the reaction of n-heptane with oxygen, the mass stoichiometric coefficient is $\nu = 3.52$. The values of Lewis number for n-heptane and oxygen are 1.8 and 1.0, respectively. A parametric study of reactants Lewis number is performed in order

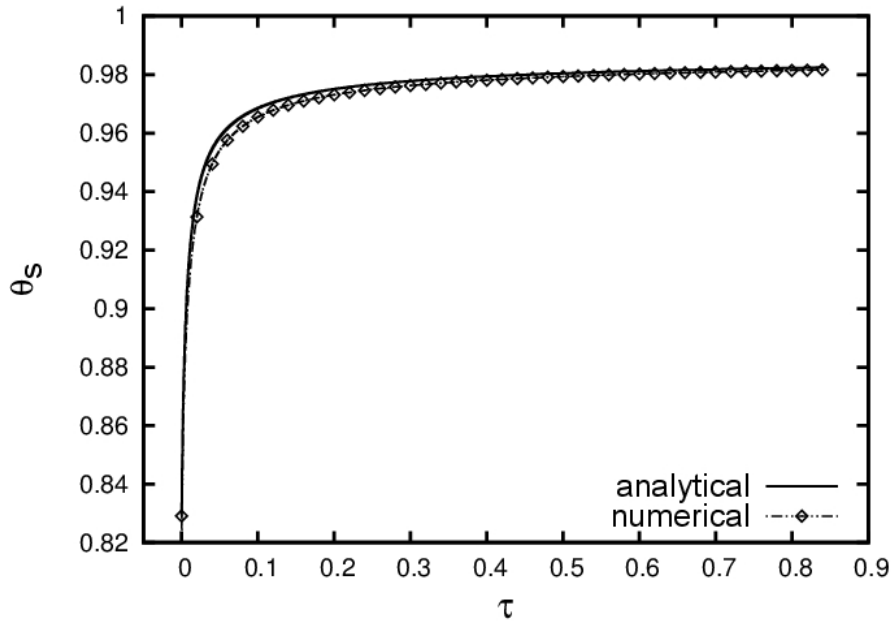


Figure 4.1 - Evolution of the droplet surface temperature as a function of time for $f \ll 1$ (comparison of analytical and numerical solutions).

to evaluate their influence on the droplet combustion under magneto relaxation heating. The volume fraction of maghemite (γFe_2O_3) nanoparticles is $\phi = 0.07$, the nanoparticle radius is $r_N = 10 \text{ nm}$, the thickness of coating layer is $\delta = 1 \text{ nm}$ and the domain of magnetization is $M_d = 414 \text{ kA/m}$. The magnetic field induction is $B_0 = \mu_0 H_0 = 1 \text{ Tesla}$.

The magnetic parameter P_m is a function of the properties of the magnetic nanoparticles, the external magnetic field and the droplet problem. Once the nanoparticle properties are specified and the fluid is chosen, the value of P_m is obtained. The conditions described above lead to $P_m = 100$. The radius variation is then practically negligible, with $a = 1 - O(P_m^{-1})$, according to Eq. (4.4). This means that the droplet heating process occurs in a short time period, $t = O(P_m^{-1})$, as previously mentioned, with no significant variation on the droplet radius. Thus, the changes in particle concentration due to evaporation, hence in magnetic susceptibility, are negligible even in the boundary layer, under the current conditions ($P_m \gg 1$). As mentioned before, the heating process occurs in a very short time and ends just before the temperature reaches the boiling temperature anywhere in the thermal boundary layer.

Figure 4.2 shows the heating time τ_h as a function of the magnetic field frequency f for different values of fuel and oxidant Lewis numbers. The heating time shown

is evaluated at the instant when the boiling temperature is reached anywhere in the boundary layer. It is verified that by increasing the magnetic field frequency, the alternating magnetic field provides more energy to the ferrofluid droplet, and as a result, the droplet heating time is reduced by about eight times. However, the relaxation process of nanoparticles reaches a saturation for $f > 3.5$. The process of alignment and misalignment starts taking longer than the period of the magnetic field, and the energy generation by viscous dissipation reaches a limit. Comparing the orders of magnitude of the various terms of Eq. (4.2), it is clear that the thermal boundary layer model becomes inappropriate when $f < 0.2$ because $f^2 P_m/A = O(1)$. Despite the limitation of the model for low frequencies, the results for $f < 0.5$ show that the heating time rises exponentially, providing evidence of the strong influence of magnetic heating on the droplet problem. Also, from Fig. 4.2, the influence of reactant Lewis number on the heating time is quantified. As expected, in conditions dominated by magnetic heating, the heat flux from the gas phase only has a slight effect on the liquid phase heating time. Thus the Lewis number only has a minor effect. The two curves below the adiabatic one ($Le_F = Le_O = 1.0$) correspond to $(Le_F = 2.0, Le_O = 1.0)$ and $(Le_F = 1.0, Le_O = 0.5)$. The other two curves, above the adiabatic one, correspond to $(Le_F = 0.5, Le_O = 1.0)$ and $(Le_F = 1.0, Le_O = 2.0)$.

Figure 4.3 shows temperature profiles in the thermal boundary layer for the limit

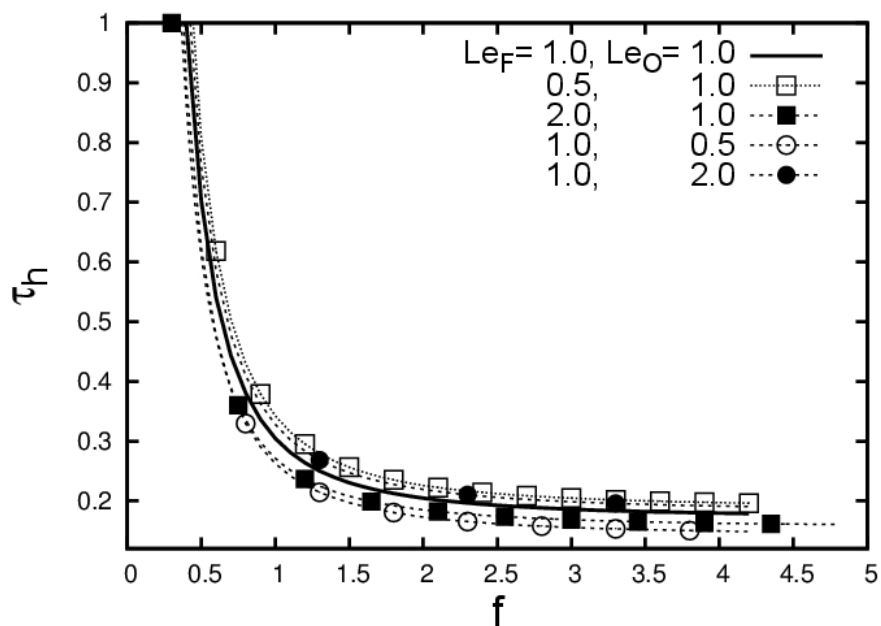


Figure 4.2 - Heating time τ_h as a function of magnetic field frequency for different values of Lewis number.

of the model $f = 0.3$, for fuel and oxidant Lewis numbers equal to 1.8 and 1.1, respectively. Temperatures inside the thermal boundary layer higher than that of

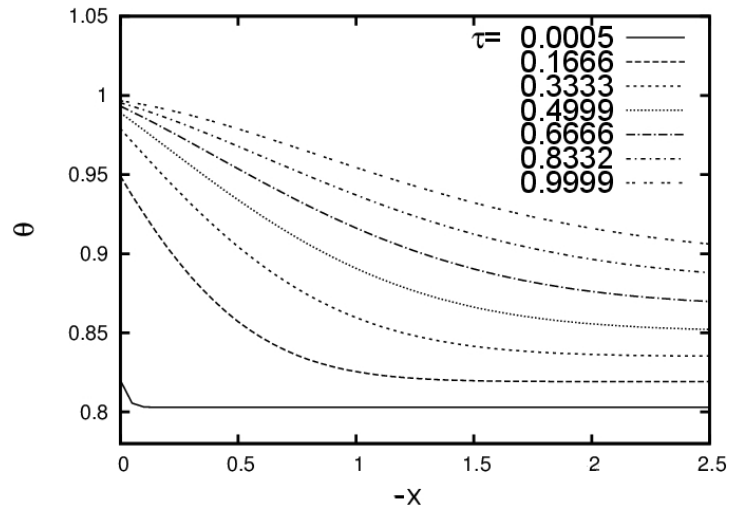


Figure 4.3 - Temperature profile of ferrofluid droplet (n-heptane) for $f = 0.3$

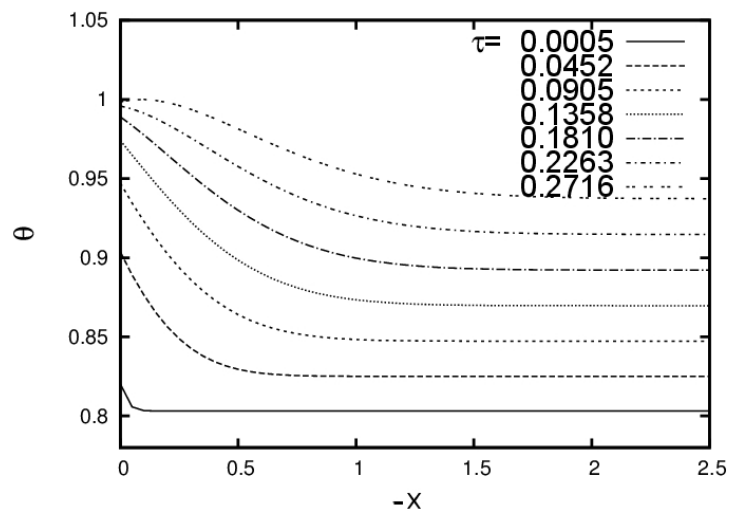


Figure 4.4 - Temperature profile of ferrofluid droplet (n-heptane) for $f = 1.0$

the droplet surface are observed in the final part of the droplet heating process. That final period is defined as occurring when the boiling temperature is reached at any part of the droplet. That high temperature ($\theta > \theta_s$) can occur because the heat flux from the flame is large enough to sustain high temperatures in the thermal boundary layer even with vaporization, which results in a decrease in temperature by

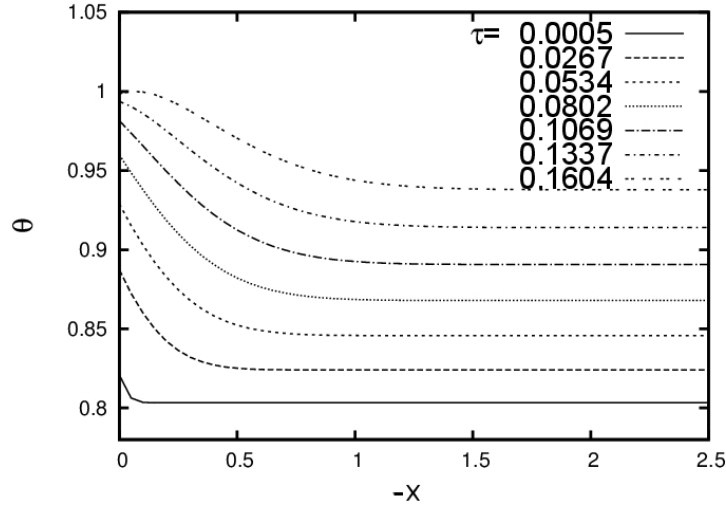


Figure 4.5 - Temperature profile of ferrofluid droplet (n-heptane) for $f = 5.0$

mass loss. Under that condition, the magnetic source, which depends upon the local temperature, can produce an increase in the thermal boundary layer temperature to values higher than that at the droplet surface. Such a result was also observed in previous works, where the interior of a semi-transparent droplet is heated under the influence of thermal radiation absorption (MILIAUSKAS, 2001; TSENG; VISKANTA, 2006).

Figures 4.4 and 4.5 show the temperature profiles for $f = 1$ and 5, respectively. Comparing Figs 4.3 to 4.5, a considerable reduction in the heating time (from 1.631 to 0.1659) is observed. Also, the thermal boundary layer thickness (from 2.347 to 0.7269) is smaller at higher frequency. The reason for this behavior is that the short heating time at high frequencies does not allow for the heat flux coming from the gas phase to reach regions deeper in the droplet core. The reduction in boundary layer thickness with frequency increase is explicitly quantified in Fig. 4.6. The result shown is obtained at the instant when the droplet reaches the boiling temperature, i.e., when the boundary layer thickness is maximum. For the conditions ($Le_F = 0.5$, $Le_O = 1.0$) and ($Le_F = 1.0$, $Le_O = 2.0$) the boundary layer thickness is less than that in adiabatic condition ($Le_F = Le_O = 1$). On the other hand, the conditions ($Le_F = 2.0$, $Le_O = 1.0$) and ($Le_F = 1.0$, $Le_O = 0.5$) leads to a boundary layer thickness larger than that in the adiabatic condition. This is because of the larger heat transfer from the gas phase for $Le_F > 1$. For a short heating time, there is no sufficient time for heat to be transferred deeper into the droplet, which results is a thinner thermal boundary layer, as seen in Fig. 4.6. In addition, the thinner thermal boundary layer thickness forces boiling to occur closer to the droplet surface. Unlike

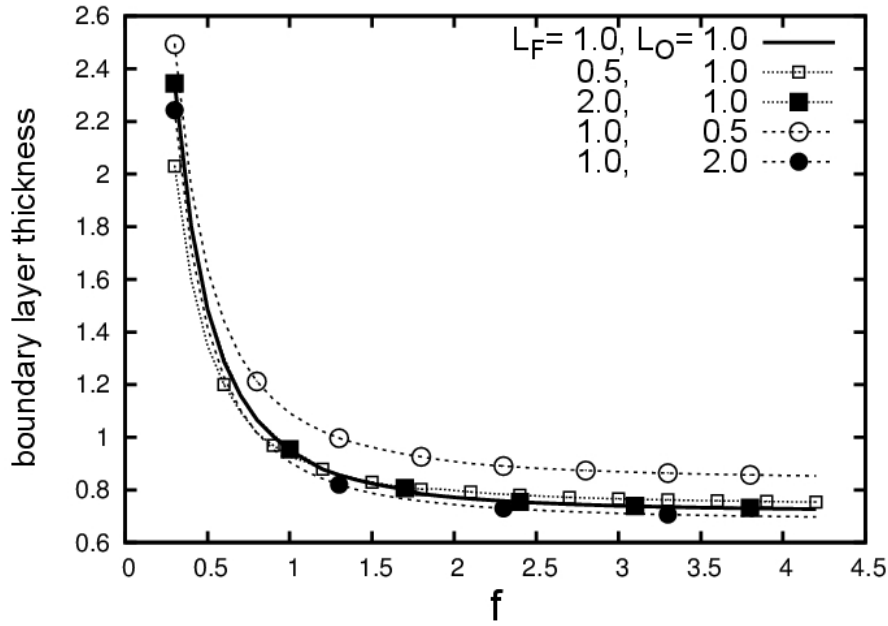


Figure 4.6 - Thermal boundary layer thickness as a function of the magnetic field frequency at the instant when boiling temperature is reached.

the effect of the fuel Lewis number, an increase of the oxidant Lewis number results in a decrease of the heat flux from the gas phase to the droplet surface. The reason for that is the reduction of the flame temperature because the heat conduction is then faster than mass diffusion. As Le_O increases, the heat flux decreases, the heating time increases (Fig. 4.2) and the thermal boundary layer thickness increases (Fig. 4.6).

Next, the dimensionless vaporization function β converted into a form suitable for comparison with experimental data, $R \equiv 8\alpha_\infty\rho_\infty^*\beta/\rho_l^*$ (GODSAVE, 1953; LAW, 1982), is shown. Figure 4.7 shows the vaporization rate R at the instant when the boiling temperature is first reached in the thermal boundary layer, as a function of magnetic field frequency for different values for Lewis number. Experimental results for n-heptane droplet burning without nanoparticles show that $R = 0.78 \text{ mm}^2/\text{s}$ when the droplet reaches the boiling temperature (KUMAGAI. et al., 1971; OKAJIMA, 1975). All results for R obtained by the present model are higher than that obtained experimentally, except the case ($Le_F = 1.0, Le_O = 2.0$), for which $R \sim 0.9 \text{ mm}^2/\text{s}$. The results show that by increasing the frequency of the magnetic field, the vaporization rate increase. The present model predicts that the vaporization may be increased up to 15% with the magnetic field frequency for the cases ($Le_F = 1.0, Le_O = 1.0$) and ($Le_F = 0.5, Le_O = 1.0$). For other cases, no significant variation with f is ob-

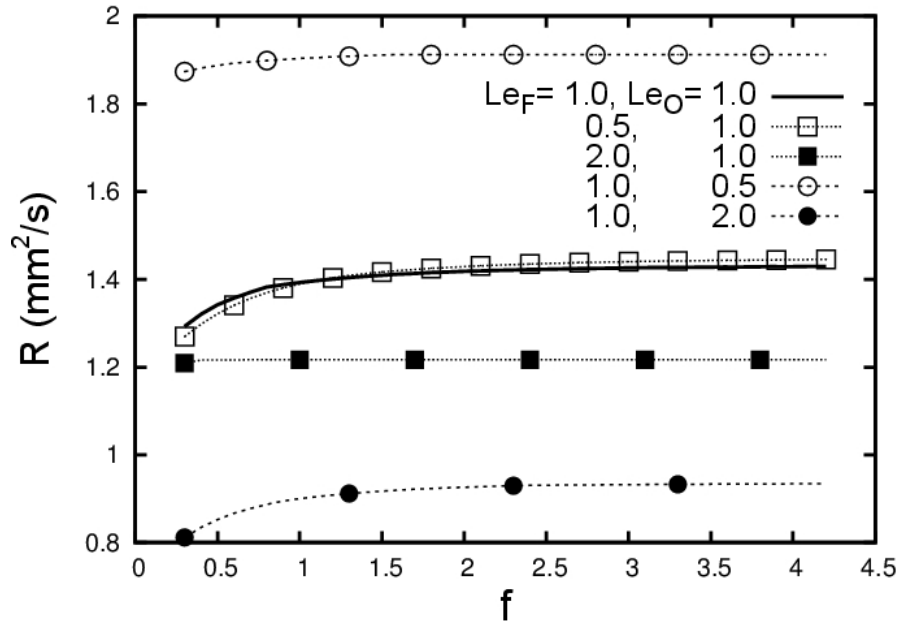


Figure 4.7 - Vaporization rate as a function of magnetic field frequency at the instant when boiling temperature is reached.

served. Changing the values of Le_F and Le_O , the vaporization rate changes from $R \sim 0.9 \text{ mm}^2/\text{s}$ to about $2 \text{ mm}^2/\text{s}$. This behavior is caused by the increase on the heat transfer provided by the transport coefficient and by increase in the flame temperature.

Although the flame temperature and the flame position are overestimated as a result of the infinite Damköhler number assumption, they are shown as a function of the magnetic field frequency, giving some qualitative measure of the influence of the magnetic heating. Figure 4.8 shows the flame temperature as a function of the alternating magnetic field frequency for different values of the fuel Lewis number. The most significant dependence of the flame temperature is on the oxidant Lewis number, as already exhibited by the classical model (FACHINI; LINÁN, 1999). For $Le_O < 1$, the diffusivity of the oxidant exceeds that of heat, consequently, to maintain the diffusive enthalpy balance in the region $r_f < r < r_\infty$, it is necessary to increase the flame temperature. Conversely, for $Le_O > 1$, the flame temperature decreases, as shown in fig 4.8. The flame temperature varies very little by changing the frequency of the external magnetic field. This result proves that the magnetic heating is practically restricted to the liquid phase.

Figure 4.9 shows the flame position as a function of the magnetic field frequency at the instant when boiling first occurs anywhere in the droplet. Different values of

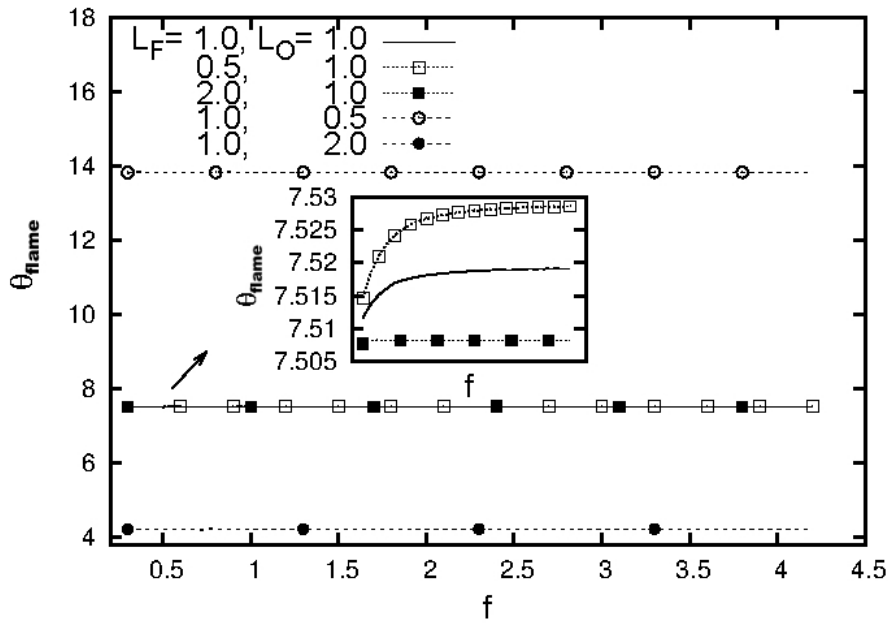


Figure 4.8 - Flame temperature as a function of magnetic field frequency at the instant when boiling temperature is reached.

the Lewis number are considered. Again it is worth remembering that the classical infinite Damköhler number model does not provide a good estimate for the flame position. However, that property is shown here because it provides some qualitative measure of the influence of magnetic heating. The results show that the flame position is strongly dependent on the oxidant Lewis number but only slightly on the fuel Lewis number (WILLIAMS, 1985; LINÁN, 1993; FACHINI; LINÁN, 1999). When the oxidant Lewis number varies from 0.5 to 2.0 (the diffusion coefficient of oxidant decreases in relation to the conductivity), the flame moves toward the oxidant. The flame position shows a clear dependence on frequency, mainly for $Le_O > 1$. When frequency increases, the flame position moves further away from the droplet because of the increase in vaporization rate.

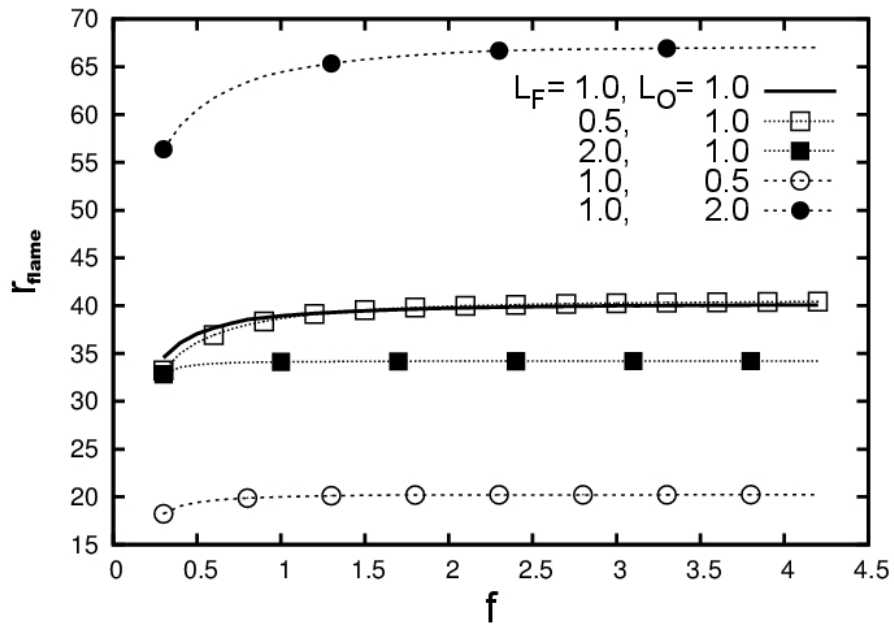


Figure 4.9 - Flame position as a function of magnetic field frequency at the instant when boiling temperature is reached.

5 CONCLUSION AND FUTURE WORKS

5.1 Conclusion

The main concern of this study is to investigate the influence of an external alternating magnetic field, via magneto relaxation, on heating, vaporization and combustion of a single ferrofluid droplet. An asymptotic analysis is performed under the condition of very large magnetic power ($P_m \gg 1$). A thermal boundary layer is established in the liquid-phase adjacent to the droplet surface due to heat flux from the ambient atmosphere. The temperature profile inside the thermal boundary layer is obtained in appropriate time and length scales. Thus, temperature profile of liquid and gas phases are matched satisfying the boundary conditions at the droplet surface.

Droplet heating is addressed in two different conditions: with combustion and without combustion. In both cases, the magnetic energy source is responsible for heating uniformly the droplet interior. The heat flux from the ambient atmosphere is responsible to change the temperature profile only in a very thin layer close the surface, in which a thermal boundary layer is observed. The combined heat sources (magnetic and thermal) inside the thermal boundary layer reduce the droplet heating time and increase the vaporization rate.

It is foreseen, since soot formation is linked directly to the overall droplet lifetime, a reduction of the droplet heating time will reduce soot emission (KESTEN et al., 1980; JACKSON; AVEDISIAN, 1994). Also, an increase in vaporization rate will allow for the development of shorter combustion chambers. The mild increase on the vaporization rate ($\sim 15\%$) leads to mild changes on the temperature and position of the flame in combustion chamber problems.

In terms of an isolated droplet problem, an increase in vaporization rate results in moderate changes on the temperature profile but has a significant effect on flame position.

The magnetic heating process of the droplet allowed that the boiling temperature occurs in the interior of the thermal boundary layer, but not at the droplet surface. Although this analysis can not follow the heating process after the thermal boundary layer to reach the boiling temperature, it is possible to foresee bubble formation inside the droplet which will break the droplet up into smaller droplets. Therefore, the magneto relaxation heating can be used in the future to improve also the atomization of fuels.

The results showed that the droplet surface temperature and the vaporization rate are influenced by changes on the fuel and oxidant Lewis numbers. Decreasing the fuel Lewis number, the vaporization rate increase and, consequently a decrease in the droplet surface temperature due to heat loss by vaporization is observed. Of course, increasing the Lewis number the droplet surface temperature increases and the vaporization rate decreases. These behaviors for vaporization rate and surface temperature favor the droplet to reach quickly the boiling temperature.

A difference between the two models (without/with combustion) is the oxidant that appears only in the case of heating with combustion. The results showed that properties such as, vaporization rate, flame temperature, flame position are strongly dependent on the oxidant Lewis number. But the influence of magnetic field frequency is evidenced only for vaporization rate and flame position, under condition of $Le_O > 1$.

By comparing the heating process of the droplet produced by the magneto relaxation and laser, advantages of the magnetic heating process is obtained. For the same droplet heating time, the magneto relaxation demands less energy and is able to heat up all droplets of the spray, meanwhile the laser heats up those droplets only inside the laser beam.

5.2 Future Works

The results presented in this work are based on the asymptotic limit of $P_m \gg 1$. This condition demands magnetic fields with very large intensity, which is produced only by special magnets. To complete the analysis of that limit, some studies will be still performed. After that, cases corresponding to $P_m = O(1)$, which is achieved by normal magnets, will be analyzed.

In the following, suggestions for future analyses covering those ideas are presented:

- It will be considered that the droplet heating time is of the same order of the characteristic time of the gas phase. Then, the transient processes from the gas phase will be accounted for together with magnetic one in the droplet heating. In terms of the dimensionless parameters, this case corresponds to $\varepsilon P_m = O(1)$. The quasi-steady model for the gas phase is not valid under this condition.
- The effect of the nanoparticles on a effective thermal conductivity will be considered. The hypothesis of thermal boundary layer should not be valid in some cases now analyzed. A more realistic model will be obtained with the inclusion of this issue.

- Cases of $P_m = O(1)$, will be considered. Then the hypothesis of constant radius will be not valid because $da/d\tau \sim P_m^{-1}$. Droplet heating occurring together with droplet vaporization is expected.
- Cases the droplet heating by the Néel relaxation mechanism, will be considered. This mechanism is predominant in base fluid with high viscosity.

Therefore, as can be seen in this work and in the suggestion of future ones, magnetic heating of fuel droplet may open new perspectives of research and technological development.

REFERENCES

- ABRAMZOM, B.; SIRIGNANO, W. A. Droplet vaporization model for spray combustion calculations. **International Journal Heat Mass Transfer**, v. 32, p. 1605–1618, 1983. 5
- ARMSTRONG, R. L. Interactions of absorbing aerosols with intense light beams. **Applied Optics**, v. 56, p. 2142, 1984. 37, 38
- ARMSTRONG, R. L.; O'ROURKE, P. J.; ZARDECKI, A. Vaporization of irradiated droplets. **Physics of Fluids**, v. 29, p. 3573, 1986. 37, 38
- BALASUBRAMANYAM, M. S.; CHEN, C. P.; TRINH, H. P. A new finite-conductivity droplet evaporation model including liquid turbulence effect. **Journal Heat Transfer**, v. 129, p. 1082–1086, 2007. 5
- BLUMS, E.; ODENBACH, S.; MEZULIS, A.; MAIOROV, M. Soret coefficient of nanoparticles in ferrofluids in the presence of a magnetic field. **Physics of Fluids**, v. 10, p. 2155, 1998. 7
- CHANDRASEKAR, M.; SURESH, S.; BOSE, A. C. Experimental investigations and theoretical determination of thermal conductivity and viscosity of Al_2O_3 /water nanofluid. **Experimental Thermal and Fluid Science**, v. 34, p. 210–216, 2010. 15
- CHEN, C. Y.; LI, C. S. Ordered microdroplet formations of thin ferrofluid layer breakups. **Physics of Fluids**, v. 22, p. 014105, 2010. 8
- CRISTALDO, C. F. C.; FACHINI, F. F. Analysis of ferrofluid droplet combustion under very large magnetic power. **Combustion and Flame**, 2013. 1
- _____. Ferrofluid droplet heating and vaporization under very large magnetic power: A thermal boundary layer model. **Physics of Fluids**, v. 25, p. 037101, 2013. 1
- DEBYEG, P. **Polar Molecules**. New York: Dover, 1929. 12
- FACHINI, F. F. An analytical solution for the quasi-steady droplet combustion. **Combustion and Flame**, v. 116, p. 302 – 306, 1999. 21, 44, 46
- FACHINI, F. F.; BAKUZIS, A. F. Decreasing nanofluid droplet heating time with alternating magnetic fields. **Journal of Applied Physics**, v. 108, p. 084309, 2010. xi, 1, 8, 15, 17, 18, 19, 28, 30, 31, 42, 43

FACHINI, F. F.; LINÁN, A. Theory of flame histories in droplet combustion at small stoichiometric fuel-air ratios. **AIAA Journal**, v. 37, p. 1426–1435, 1999. 20, 21, 44, 46, 53, 54

FAETH, G. M. Current status of droplet and liquid combustion. **Progress in Energy and Combustion Science**, v. 3, p. 191 – 224, 1977. 1, 3, 8

FELDERHOF, B. U. Ferrohydrodynamic pumping of a ferrofluid or electrohydrodynamic pumping of a polar liquid through a circular tube. **Physics of Fluids**, v. 23, p. 092002, 2011. 7

FENG, Y.; YU, B.; XU, P.; ZOU, M. The effective thermal conductivity of nanofluids based on the nanolayer and the aggregation of nanoparticles. **Journal of Physics D: Applied Physics**, v. 40, p. 3164–3171, 2007. 6

GAN, Y.; QIAO, L. Combustion characteristics of fuel droplets with addition of nano and micron-sized aluminum particles. **Combustion and Flame**, v. 158, p. 354–368, 2011. 7, 15

_____. Evaporation characteristics of fuel droplets with the addition of nanoparticles under natural and forced convections. **International Journal in Heat Mass Transfer**, v. 54, p. 4913–4922, 2011. 7

GILCHRST, R. K.; MEDAL R. SHOREY, W. D.; HANSELMAN, R. C.; PARROT, J. C.; TAYLOR, C. B. Selective inductive heating of lymph nodes. **Annals of Surgery**, v. 146, p. 596, 1957. 8

GODSAVE, G. A. E. Studies of the combustion of drops in a fuel spray: the burning of a single drops of fuel. **Proceedings of the Combustion Institute**, v. 4, p. 818–830, 1953. 4, 52

HATCH, A.; KAMHOLZ, A.; HOLMAN, G.; YAGER, P.; BOHRINGER, K. A ferrofluidic magnetic micropump. **Journal of Microelectromechanical Systems**, v. 10, p. 215–221, 2001. 7

JACKSON, G. S.; AVEDISIAN, C. T. The effect of initial diameter in spherically symmetric droplet combustion of sooting fuels. **Proceedings of the Royal Society A**, v. 446, p. 225–276, 1994. 57

JUNG, K. M.; TING, C. C.; LIN, B. F.; TSUNG, T. T. Aqueous aluminum nanofluid combustion in diesel fuel. **Journal of Testing and Evaluation**, v. 36, p. 100579, 2008. 7

- KAPPIYOOR, R.; LIANGRUKSA, M.; GANGULY, R.; PURI, I. K. The effects of magnetic nanoparticle properties on magnetic fluid hyperthermia. **Journal of Applied Physics**, v. 108, p. 094702, 2010. 1, 8
- KESTEN, A. S.; SANGIOVANNI, J. J.; GOLDBERG, P. Conceptual examination of gas phase particulate formation in gas turbine combustion. **Journal Eng. Power**, v. 102, p. 613–618, 1980. 57
- KOTAKE, S.; OKAZAKI, T. Evaporation and combustion of fuel droplet. **International Journal Heat and Mass Transfer**, v. 12, p. 595–610, 1969. 5
- KUMAGAI, S.; SAKAI, T.; OKAJIMA, S. Experimental investigation of free droplet combustion under microgravity. **Proceedings of the Combustion Institute**, v. 13, p. 779–785, 1971. 52
- KUO, K. K. **Principles of combustion**. New York: Wiley, 1986. 2
- LAW, C. Recent advances in droplet vaporization and combustion. **Progress in Energy and Combustion Science**, v. 8, p. 171 – 201, 1982. 1, 3, 41, 52
- LAW, C. K.; SIRIGNANO, W. A. Unsteady droplet combustion with droplet heating II: conduction limit. **Combustion and Flame**, v. 28, p. 175–186, 1977. 5
- LINÁN, A. **Fluid dynamic aspects of combustion theory**. Michigan: Longman Scientific and Technical, 1991. 45
- _____. **Fluid aspects of combustion**. Oxford: Oxford University Press, 1993. 54
- _____. **Mechanics for a new millennium: Diffusion-controlled combustion**. New York: Kluwer Academic Publishers, 2001. 45
- LORELL, J.; WISE, H.; CARR, R. E. Steady-state burning of a liquid droplet II: bipropellant flame. **Journal of Chemical Physics**, v. 25, p. 325, 1956. 2
- MAENOSONO, S.; SAITA, S. Theoretical assessment of *FePt* nanoparticles as heating elements for magnetic hyperthermia. **Magnetics, IEEE Transactions on**, v. 42, p. 1638–1642, 2006. 43
- MILIAUSKAS, G. Regularities of unsteady radiative conductive heat transfer in evaporating semitransparent liquid droplets. **International Journal Heat Mass Transfer**, v. 44, p. 785–798, 2001. 51
- ODENBACH, S. **Ferrofluids: magnetically controllable fluids and their applications**. Berlin: Springer, 2002. 6

_____. **Colloidal magnetic fluids**. Berlin: Springer, 2009. 6, 8

OKAJIMA, S. K. S. Further investigations of combustion of free droplets in a freely falling chamber including moving droplets. **Proceedings of the Combustion Institute**, v. 15, p. 401–407, 1975. 52

ONDECK, C. L.; HABIB, A. H.; OHODNICKI, P.; MILLER, K.; SAWYER, C. A.; CHAUDHARY, P.; MCHENRY, M. Theory of magnetic fluid heating with an alternating magnetic field with temperature dependent materials properties for self-regulated heating. **Journal of Applied Physics**, v. 105, p. 07B324–07B324, 2009. 7, 14

PARK, B. S.; ARMSTRONG, R. L. Laser droplet heating: fast and slow heating regimes. **Applied Optics**, v. 28, p. 3671, 1989. xii, 37, 38, 39, 40

PEYGHAMBARZADEH, S.; HASHEMABADI, S.; JAMNANI, M. S.; HOSEINI, S. Improving the cooling performance of automobile radiator with Al_2O_3 /water nanofluid. **Applied Thermal Engineering**, v. 31, n. 10, p. 1833–1838, 2011. 6

PLAZA, J. A.; ESTEVE, J.; LOSANTOS, P.; ACERO, M. C.; CANE, C. The use of ferrofluids in micromechanics. **Sensors and Actuators**, p. 176–180, 2000. 7

PRAKASH, S.; SIRIGNANO, W. A. Liquid fuel droplet heating with internal circulation. **International Journal Heat Mass Transfer**, v. 21, p. 885–895, 1978. 5

_____. Theory of convective droplet vaporization with unsteady heat transfer in the circulating liquid phase. **International Journal Heat Mass Transfer**, v. 23, p. 253–268, 1980. 5

RAJA, S.; DEVI, G.; KARTHIKEYAN, M. Nanofluid applications in future automobiles: comprehensive review of existing data. **Nano-Micro Letters**, v. 2, p. 306–310, 2011. 7

ROSENSWEIG, R. Heating magnetic fluid with alternating magnetic field. **Journal of Magnetism and Magnetic Materials**, v. 252, p. 370–374, 2002. 1, 6, 8, 11, 13, 18

ROSENSWEIG, R. E. **Ferrohydrodynamics**. New York: Cambridge University Press, 1985. 6, 7, 12, 13, 14

SARIT, K. D.; STEPHEN, U. S. C.; WENHUA, Y.; PRADEEP, T. **Nanofluids: science and technology**. New Jersey: Wiley, 2007. 6

SAZHIN, S. S. Advanced models of fuel droplet heating and evaporation. **Progress in Energy and Combustion Science**, v. 32, n. 2, p. 162 – 214, 2006. 1, 3, 8

SHAFII, M. B.; DANESHVAR, F.; JAHANI, N.; MOBINI, K. Effect of ferrofluid on the performance and emission patterns of a four-stroke diesel engine. **Advances in Mechanical Engineering**, v. 2011, p. 1–5, 2011. 7

SHLIOMIS, M. Ferrohydrodynamics: Retrospective and issues. **Ferrofluids**, Springer, p. 85–111, 2003. 6, 7

SINGH, D.; TOUTBOURT, J.; CHEN, G. Heavy vehicle systems optimization merit review and peer evaluation. **Annual Report Argonne National Laboratory**, 2006. 6

SIRIGNANO, W. Fuel droplet vaporization and spray combustion theory. **Progress in Energy and Combustion Science**, v. 9, p. 291–322, 1983. 3, 5, 8, 41

SIRIGNANO, W. A. **Fluid dynamics and transport of droplets and sprays**. New York: Cambridge, 1999. 3, 5

SPALDING, D. B. The combustion of liquid fuels. **Proceedings of the Combustion Institute**, v. 4, p. 847–864, 1953. 4

TILLMAN, P.; HILL, J. Determination of nanolayer thickness for a nanofluid. **International Communications in Heat and Mass Transfer**, v. 34, p. 399–407, 2007. 6

TSENG, C. C.; VISKANTA, R. Enhancement of water droplet evaporation by radiation absorption. **Fire Safety Journal**, v. 41, p. 236–247, 2006. 9, 28, 51

TYAGI, H.; PHELAN, P.; PRASHER, R.; PECK, R.; LEE, T.; PACHECO, J.; ARENTZEN, P. Increased hot-plate ignition probability for nanoparticle-laden diesel fuel. **Nano Letters**, v. 8, p. 1410–1416, 2008. 7

UMEMURA, A. Interactive droplet vaporization and combustion: approach from asymptotics. **Proceedings of the Combustion Institute**, v. 20, p. 325–372, 1994. 3

VEKAS, L. Magnetic nanoparticles and concentrated magnetic nanofluids: synthesis, properties and some applications. **China Particuology**, v. 5, p. 43–49, 2007. 7

VÖLKER, T.; ODENBACH, S. The influence of a uniform magnetic field on the solet coefficient of magnetic nanoparticles. **Physics of Fluids**, v. 15, p. 2198, 2003. 7

WALDMAN, C. H. Theory of non-steady state droplet combustion. **Proceedings of the Combustion Institute**, v. 15, p. 429–442, 1975. 42

WANG, B. A fractal model for predicting the effective thermal conductivity of liquid with suspension of nanoparticles. **International Journal of Heat and Mass Transfer**, v. 46, p. 2665–2672, 2003. 6

WEN, D.; LIN, G.; VAFAEI, S.; ZHANG, K. Review of nanofluids for heat transfer applications. **Particuology**, v. 7, p. 141–150, 2009. 6

WILLIAMS, F. A. On the assumptions underlying droplet vaporization and combustion theories. **Journal of Chemical Physics**, v. 33, p. 133, 1960. 5

_____. **Combustion theory: the fundamental theory of chemically reacting flow systems**. Menlo Park, CA: Benjamin, 1985. 54

WISE, H.; ABLOW, C. M. Burning of a liquid droplet III: conductive heat transfer within the condensed phase during combustion. **Journal of Chemical Physics**, v. 27, p. 389, 1957. 4, 5

WONG, K. V.; LEON, O. D. Applications of nanofluids: current and future. **Advances in Mechanical Engineering**, v. 2010, p. 1–11, 2010. 6

XUAN, Y. Heat transfer enhancement of nanofluids. **International Journal of Heat and Fluid Flow**, v. 21, p. 58–64, 2000. 6

XUAN, Y.; ROETZEL, W. Conceptions for heat transfer correlation of nanofluids. **Heat and Mass Transfer**, v. 43, p. 3701–3707, 2000. 6

XUE, Q.-Z. Model for effective thermal conductivity of nanofluids. **Physics Letters A**, v. 307, p. 313–317, 2003. 6, 15

YAMAHATA, C.; CHASTELLAIN, M.; PARASHAR, V.; PETRI, a.; HOFMANN, H.; GIJS, M. Plastic micropump with ferrofluidic actuation. **Journal of Microelectromechanical Systems**, v. 14, p. 96–102, 2005. 7

YU, W. The role of interfacial layers in the enhanced thermal conductivity of nanofluids: a renovated maxwell model. **Journal of Nanoparticle Research**, v. 5, p. 167–171, 2003. 6

ZHANG, Y.; MA, H. Nonequilibrium heat conduction in a nanofluid layer with periodic heat flux. **International Journal of Heat and Mass Transfer**, v. 51, p. 4862–4874, 2008. 6

PUBLICAÇÕES TÉCNICO-CIENTÍFICAS EDITADAS PELO INPE

Teses e Dissertações (TDI)

Teses e Dissertações apresentadas nos Cursos de Pós-Graduação do INPE.

Manuais Técnicos (MAN)

São publicações de caráter técnico que incluem normas, procedimentos, instruções e orientações.

Notas Técnico-Científicas (NTC)

Incluem resultados preliminares de pesquisa, descrição de equipamentos, descrição e ou documentação de programas de computador, descrição de sistemas e experimentos, apresentação de testes, dados, atlas, e documentação de projetos de engenharia.

Relatórios de Pesquisa (RPQ)

Reportam resultados ou progressos de pesquisas tanto de natureza técnica quanto científica, cujo nível seja compatível com o de uma publicação em periódico nacional ou internacional.

Propostas e Relatórios de Projetos (PRP)

São propostas de projetos técnico-científicos e relatórios de acompanhamento de projetos, atividades e convênios.

Publicações Didáticas (PUD)

Incluem apostilas, notas de aula e manuais didáticos.

Publicações Seriadas

São os seriados técnico-científicos: boletins, periódicos, anuários e anais de eventos (simpósios e congressos). Constam destas publicações o Internacional Standard Serial Number (ISSN), que é um código único e definitivo para identificação de títulos de seriados.

Programas de Computador (PDC)

São a seqüência de instruções ou códigos, expressos em uma linguagem de programação compilada ou interpretada, a ser executada por um computador para alcançar um determinado objetivo. Aceitam-se tanto programas fonte quanto os executáveis.

Pré-publicações (PRE)

Todos os artigos publicados em periódicos, anais e como capítulos de livros.